Optimizing AFP Manufactured Composite-Based Cryogenic Tanks for Space-Based Missions

Matthew T. Nuss

A thesis
submitted in partial fulfillment of the
requirements for the degree of

Master of Science

University of Washington

2024

Committee:

Marco Salviato

Jeff Wollschlager

Program Authorized to Offer Degree:
Department of Aeronautics & Astronautics

University of Washington

Abstract

Optimizing AFP Manufactured Composite-Based
Cryogenic Tanks for Space-Based Missions

Matthew T. Nuss

Co-Chairs of the Supervisory Committee:
Marco Salviato
Aeronautics and Astronautics

Jeff Wollschlager
Aeronautics and Astronautics

When going into space, rockets need to keep their liquid hydrogen fuel at a very low temperature to maintain its liquid state and minimize the amount that boils away and escapes. This means its propellant tank must have good mechanical properties at incredibly low temperatures. Yet there is an added challenge when going into space; this fuel is not cheap by any stretch of the imagination. Carbon fiber has become a very popular material in the aerospace industry for its fantastic mechanical properties [1] and exceptional weight-to-strength ratio [2].

In this thesis, we will look at designing and optimizing a cryogenic rocket propellant tank made completely out of Carbon Fiber Reinforced Composite (CFRC) to make it as strong as necessary yet as light as possible. These structures are not often optimized in very rigorous detail, missing out on what can be significant weight savings for the structure and in turn the entire rocket. Structures such as this are optimized via state-of-the-art software and compared to traditional design both in terms of performance and manufacturability. Three different optimized layups are introduced and compared to a benchmark industry design in terms of their weights, mechanical strengths, and abilities to be manufactured using automatic fiber placement (AFP).

TABLE OF CONTENTS

LIST OF FIGURES

GLOSSARY

COMPOSITE: A material made out of a combination of two or more materials.

CARBON FIBER REINFORCED COMPOSITE (CFRC): Composite made of a matrix material, typically epoxy, reinforced with strands of carbon fiber.

TOW: A single strand of a composite material that is laid down in the manufacturing process.

PLY: A single layer of a composite material, made of many tows laid together to make a sheet.

PLY ORIENTATION: Direction a ply points based on its fiber direction relative to some defined axis, usually along the length of the structure. The direction along the length of a fiber strand is considered the 1-direction. Two spatial directions that make a plane transverse to the 1-direction define the 2- and 3-directions.

LAMINATE: Plies of CFRC stacked on top of one another to make some sort of structure.

YOUNG'S MODULUS (E): Measure of the ability of a material to withstand changes in length when being pulled or compressed.

SHEAR MODULUS (G): Measure of the ability of a material to resist deformation when experiencing a force parallel to one of its faces while its opposite face experiences an opposing force.

POISSON'S RATIO (ν): Measure of the deformation of a material in directions perpendicular to the specific direction of loading, also called Poisson's Effect.

COMPLIANCE: The inverse of stiffness in engineering. The higher the compliance, the more a structure displaces when loaded.

AUTOMATED FIBER PLACEMENT (AFP): One process for making composite structures where a machine lays down tows of CFRC to make a larger structure.

CRYOTANK: A portmanteau word combining "cryogenic" and "tank." A tank is said to be a cryotank when it hold cryogenic fuel, or fuel that is only liquid at very cold temperatures.

LAYUP: The way the carbon fiber tows are laid down. This includes orientation, the order of individual plies stacked together, and amount of each type of ply orientation.

ANISOTROPY: Material whose properties vary in different directions.

STRESS/STRAIN ALLOWABLES: In Hyperworks, the material property values input in the Material Card that define the maximum stress value that the property can withstand before failure. Stress values are often found using studies such as those composed by NIAR and strain allowable can be calculated simply using $\varepsilon = E\sigma$.

Z_O OFFSET: The distance in a laminate from the shell surface to the bottom of the first ply.

STACKING SEQUENCE: Specific order in which plies are laid in a laminate. Structures' final mechanical properties are often dependent on the stacking sequence.

SMEAR: Computational and mathematical concept in composites in which plies are homogenized through the thickness of the stacked laminate to make the laminate independent of stacking sequence.

OPTIMIZATION: The process in engineering of using specific design constraints to meet a design objective for a structure, such as trying to reduce mass as much as possible based on material failure criteria.

DESIGN VARIABLES: In optimization problem definition, things that can change in the model, such as thickness. The **D** in **DRCO**.

RESPONSES: In optimization problem definition, values measured from model changes, such as allowable stress. The **R** in **DRCO**.

CONSTRAINTS: In optimization problem definition, limits on responses of the model that must be satisfied. The **C** in **DRCO**.

OBJECTIVES: In optimization problem definition, a single response of the model to be minimized or maximized, such as the mass. The **O** in **DRCO**.

FACTOR OF SAFETY (FOS): Value introduced to make a structure stronger than may be absolutely necessary. A FOS of 1.5 means making a tank that can withstand 0.375 MPa of internal pressure even though it will only experience 0.25 MPa of internal pressure.

HOOP WINDING: Fiber tow winding about a pressure vessel that is perpendicular to the length of the vessel, $\alpha \simeq 90°$.

AXIAL WINDING: Fiber two winding about a pressure vessel along the length of the vessel, $\alpha = 0°$.

HELICAL WINDING: Fiber tow winding about a pressure vessel that is neither parallel or perpendicular to the length of the vessel. Classified between Low-Angle Helical Winding ($0°45°$) and High Angle Helical Winding ($45°90°$).

ACKNOWLEDGMENTS

I would like to express my deepest gratitude to my advisor, Dr. Marco Salviato, for his invaluable guidance and patience. Many thanks also to my advisor Jeff Wollschlager, for mentoring me on the ins and outs of Optistruct as well as composite modelling and manufacturing. Also, a special thank you to Kameron Harmon for the help in confirming the manufacturability of these models.

Chapter 1

INTRODUCTION

When going into space, rockets need to keep their liquid hydrogen fuel at a very low temperature to maintain its liquid state and minimize the amount that boils away and escapes. This means its propellant tank must have good mechanical properties at incredibly low temperatures. Yet there is an added challenge when going into space; this fuel is not cheap by any stretch of the imagination. Shedding weight in any way possible means it can be that much easier and cheaper to reach space, a difficult and expensive endeavor. Carbon fiber has become a very popular material in the aerospace industry. One, for its fantastic mechanical properties [1]. Two, for its ability to be manufactured *ad hoc* for the specific application they are intended to [7]. And three, for its exceptional weight-to-strength ratio, especially in comparison to traditional steel [2].

In this thesis, we will look at designing and optimizing a cryogenic rocket propellant tank made completely out of Carbon Fiber Reinforced Composite (CFRC). This tank will be as strong as possible yet as light as necessary for use in space missions while maintaining the ability to be manufactured. Structures are optimized via state-of-the-art software and compared to traditional design both in terms of performance and manufacturability. Three different optimized layups are introduced and compared to a benchmark industry design under the same loads to compare their weights, mechanical strengths, and abilities to be manufactured using automatic fiber placement (AFP).

1.1 Composites for Aerospace Applications

A composite material is a combination of two or more materials with different physical properties such as stiffness and strength [8]. Different materials can be combined to take advantage of individual properties they have to obtain a"new" material with certain properties for specific uses. In this thesis, the material we will concern ourselves with is carbon

fiber reinforced composites (CFRC). These are typically stretchy epoxy matrices reinforced with strong carbon fibers for added structure and strength. Epoxy is used as the matrix for its low density and ability to resist change to dimensions when stretched or compressed. Meanwhile, carbon fibers are useful for their high strength and stiffness. When combined to make CFRCs such as the simple example of a single ply in figure 1.1, they make exceptionally strong materials while remaining incredibly light. This means we can use less material that is already lighter than traditional steel to make aerospace structures; such as a rocket fuel tank like the one made by Rocket Lab in figure 1.2.

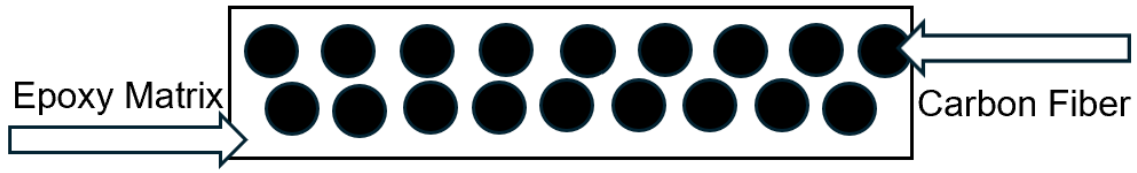

Figure 1.1: Simplified ply of carbon fiber reinforced composite (CFRC).

When going into space, weight is everything. Lowering a structure's weight means a lighter overall payload, which means less rocket fuel is needed to go to space and thus saves a lot of money. Carbon fiber is ten times stronger than steel, yet is only a quarter of steel's weight making it a very exciting candidate for aerospace applications [1]. To put into perspective the price of burning rocket fuel, NASA bought 7.5 million pounds of liquid hydrogen in 2022 at the price of $10 per pound, or $22.04 per kilogram [9]. NASA's Space Launch System rocket holds 537,000 gallons of liquid hydrogen, equating to just over 317,000 pounds of liquid hydrogen [10]. Coming in at $10 per pound, for one rocket over $3 million of liquid hydrogen is needed to go to space. Shedding weight in any way possible, such as the tank needed to hold the rocket fuel, is paramount to saving as much money as possible on a very expensive venture.

Figure 1.2: Composite-based rocket fuel tank made by Rocket Lab [3]. This particular one is made in two parts, whereas this project will be making a tank out of one continuous part.

1.2 Properties of Composites

As briefly discussed earlier, composite materials are exceptional in aerospace applications not only for their weight, but also their mechanical properties. Because carbon fiber is so strong, CFRCs are strongest along the length of these strong carbon fibers. CFRCs are made by taking long, thin strands of carbon fiber placed side-by-side and making spools of tape by covering them with sticky epoxy resin. When combined with epoxy to make CFRCs, a few parameters are used to quantify how it will react under certain loading conditions. Most commonly used are Young's Modulus, Shear Modulus, and the Poisson Ratio.

Young's Modulus (E) is a measure of the ability of a material to withstand changes in length when being pulled or compressed. Along the length of the fiber, (the 1-direction as shown in figure 1.3) [8].

$$E_1 = V_f E_f + V_m E_m \tag{1.1}$$

Where $V_{f/m}$ represents the volume ratio of the fiber/matrix in the composite and $E_{f/m}$ is the Young's modulus of the individual fiber or matrix respectively, which are empirically known values. E transverse (perpendicular) to the length of the fiber (the 2 and 3 directions as shown in figure 1.3) is

$$\frac{1}{E_2} = \frac{V_f}{E_f} + \frac{V_m}{E_m} \tag{1.2}$$

Young's Modulus in the two and three directions are equal due to CFRCs being treated as transversely isotropic materials [8]. This means CFRCs have a plane of isotropy, the 2-3 plane such as the plane in figure 1.3 that is in the same direction as the paper you are reading on, which has material properties that are the same when perpendicular to that plane (pointing out of the page, the same direction as the carbon fiber). However, it has different material properties perpendicular to the other planes (such as the direction pointing up and down versus left and right). In 1.4, Young's Modulus is represented on the far left. As the force pulls down perpendicular to the bottom face of the unit cell, it resists being stretched as it would if it had a lower E value.

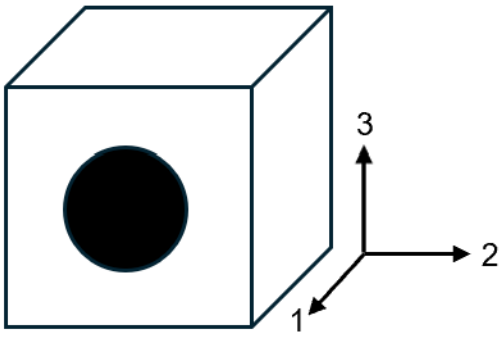

Figure 1.3: Unit cell of a carbon fiber with matrix surrounding it. The 1-axis is along the length of the fiber and the 2 and 3 axes are perpendicular to the fiber.

Shear Modulus (G) is a measure of the ability of a material to resist deformation when experiencing a force parallel to one of its faces while its opposite face experiences an opposing force. The shear modulus for a force along the length of the fiber is [8].

$$G_{12} = \left(\frac{V_f}{G_{f12}} + \frac{V_m}{G_m} \right)^{-1} = G_{13} \tag{1.3}$$

Shear modulus experiencing a force transverse to the length of the fiber is

$$G_{23} = \frac{E_2}{2(1 + \nu_{23})} = G_{32} \tag{1.4}$$

Where ν_{23} is the Poisson Ratio in the 2-3 direction [8]. In figure 1.4, Shear Modulus is represented in the middle. As the force pulls parallel to the top face of the unit cell, it resists being deformed as it would if it had a lower G value. In the case shown, the opposing force is the bottom face being rooted to the ground.

Poisson's Ratio is a measure of the deformation of a material in directions perpendicular to the specific direction of loading, also called Poisson's Effect. For ν in the direction of the fiber, $\nu_{12} = \nu_{13}$. In the directions transverse to the fiber, $\nu_{21} = \nu_{31}$ and $\nu_{23} = \nu_{32}$. Poisson Ratio's are often measured in lab and calculated using the relations with strain

$$\nu_{ij} = -\frac{d\varepsilon_j}{d\varepsilon_i} \tag{1.5}$$

and the composite's Young's Modulus

$$\frac{\nu_{ij}}{E_i} = \frac{\nu_{ji}}{E_j} \tag{1.6}$$

In figure 1.4, Poisson's Ratio is represented on the right. As the unit cell is stretched it experiences a change in strain in the longitudinal direction and lateral direction. When these strains are measured in lab, they can then be simply calculated using the equation above.

During the specific manufacturing process we will be looking at, a robot loaded with strands of CFRC lays down multiple strands at a time, called tows. This process is called Automated Fiber Placement (AFP) because instead of traditional manufacturing methods done by hand, a robot such as the one in figure 1.5 can lay the strands for us. This is a very precise and intricate process as will be seen later. When making large sheets of carbon fiber, known as plies, the tows are laid in the same direction relative to one another to make

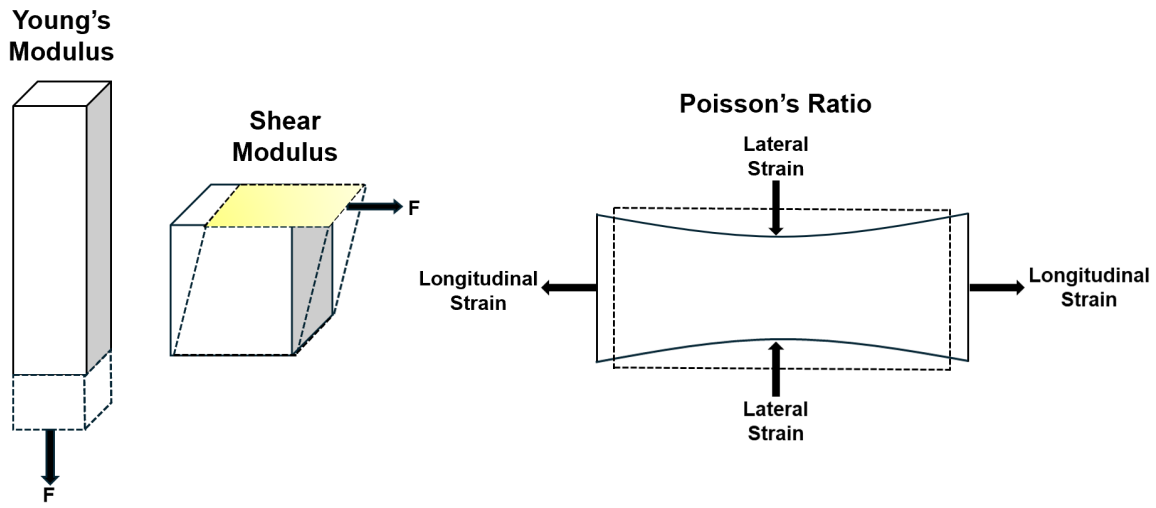

Figure 1.4: Physical examples of Young's Modulus, Shear Modulus, and Poisson's Ratio.

these plies. So a single ply of CFRC will have the same properties as a single strand of CFRC, but now as an entire sheet as opposed to a single strand.

When making composite-based structures such as the tank we will be looking at, you can stack and arrange the thin plies on top of one another in different orientations. This is advantageous because once stacked, weak points such as a ply being pulled apart transverse to the length of the fiber, is minimized by being reinforced with plies on top, such as in figure 1.6. By stacking the plies in different orientations, different overall structure properties can be achieved. Sometimes, composite plies can be stacked to deform a specific way when loaded. Other times plies can be stacked to make a structure as strong as possible. In the scope of this thesis looking at a propellant tank, the goal is to orient the tows and plies in a way to maximize strength while minimizing material used, all while keeping manufacturability in mind.

Thermal properties of CFRCs also makes this material a strong candidate for cryogenic purposes. Assuming a liquid hydrogen rocket fuel which is very common, the fuel needs to be maintained at a cryogenic temperature of -253°C [2]. Temperatures this low can have a large impact on mechanical properties. However, there are CFRCs made for extreme conditions used often in the aerospace industry. One of the most common CFRCs is Toray's T700GC

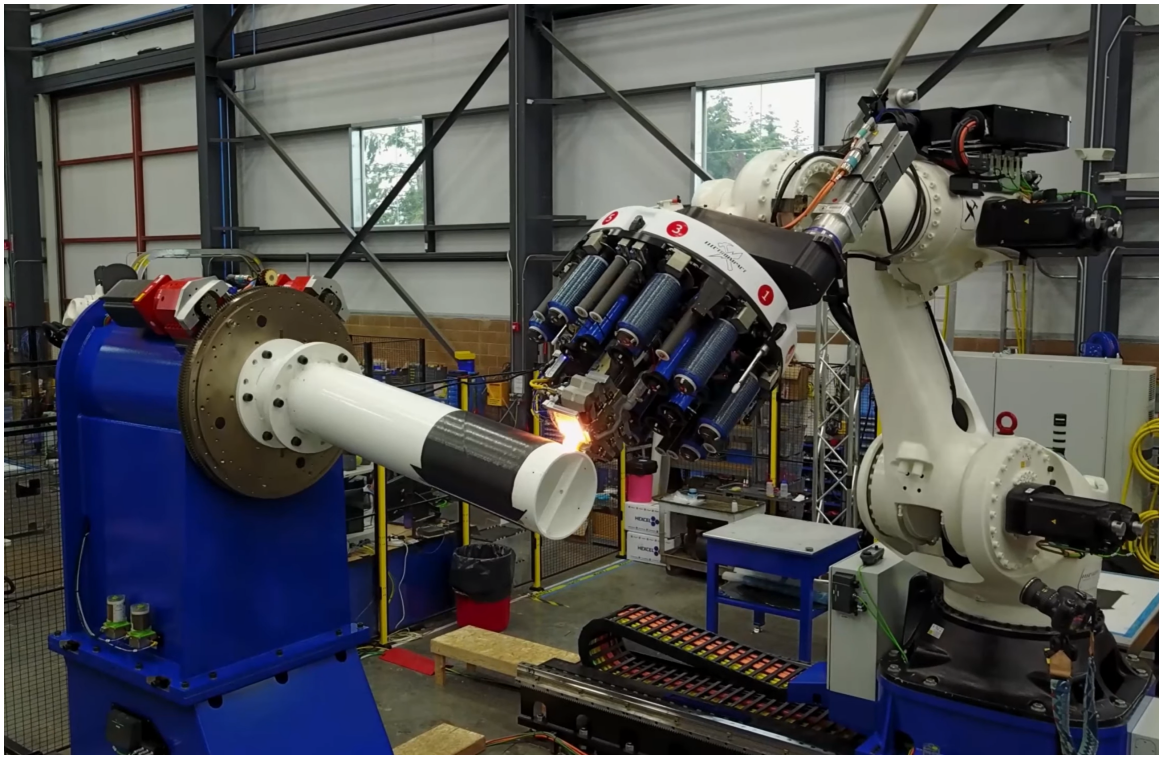

Figure 1.5: Screenshot of an AFP robot by ElectroImpact. [4]

Uni-directional tape which is the material we will be using in this thesis. This material is used often in aerospace structures because of its ability to deform without breaking and being easy to work with when manufacturing. When strength was tested at cryogenic temperatures, T700GC proved to be stronger in both tension and compression [11]. This combined with its manufacturability compatible with AFP as well as its already wide use in industry makes T700GC the ideal candidate for this broad study.

1.3 Current State of Composite-Based Cryogenic Propellant Tanks

Since the 1980s, efforts have been made to utilize composite materials into space-based cryotank applications. The first challenge came from being able to utilize a material at such extremely low temperatures without it becoming so brittle it will fail. Also, liquid hydrogen has a very fine molecular structure. Therefore there is also the challenge of preventing

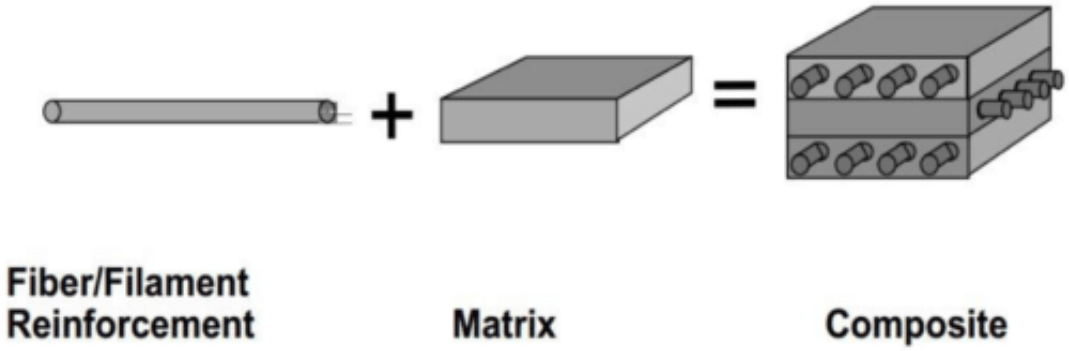

Figure 1.6: Simplified carbon fiber reinforced composite (CFRC) with multiple layers of different orientations. [5]

the fuel from escaping through the tiniest imperfections in the tank. This is especially challenging for CFRCs because they are made of thin tows, so any slight gap between tows can provide a route of escape for the hydrogen fuel [6].

Teams at companies such as Lockheed Martin, Boeing, and Northrop Grumman as well as NASA have been at the forefront of modern explorations into composite-based cryotanks. Multiple techniques are being used to add rigidity to these cryotanks, such as Lockheed Martin's external stiffening "collar" or Northrop Grumman's use of a honeycomb intermediate layer between external and internal walls as seen in figure 1.7. NASA and Boeing collaborated in 2018 using a fluted core collar for external stiffening on a 2.4 m and 5.5 m tank to advance technology and manufacturing readiness levels for full scale tanks [12]. These are all different and elegant ways to make composite-based cryotanks with the necessary structural properties for space-based applications, and all have saved weight between 25% and 42.8% [6] [12]. For this thesis, we are going to look at ways to optimize the most general case of a composite-based cryotank. No external structures or intermediate layers, strictly a tank made entirely of CFRC. This way we optimize the main part of the cryotank and later studies can look at ways to optimize further with advanced structures with an already optimized CFRC cryotank.

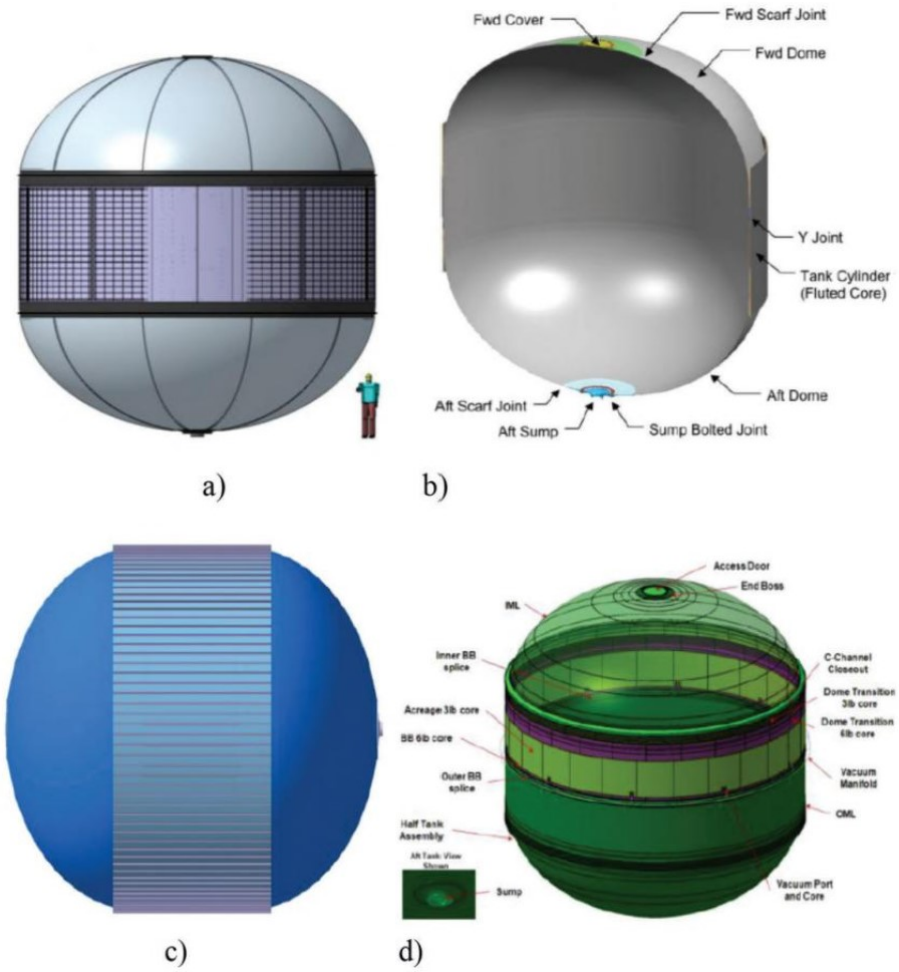

Figure 1.7: Three modern cryotanks designs. (a) NASA al-Li metallic baseline concept (not composite), (b) Boeing fluted core sandwich wall concept, (c) Lockheed Martin externally stiffened concept, and (d) Northrop Grumman composite honeycomb sandwich concept.[6]

Chapter 2

PROBLEM FORMULATION AND APPROACH

The purpose of this thesis is to take a simple model for a cryogenic propellant tank made completely of Toray's T700GC carbon fiber reinforced composite (CFRC) and optimize the layup to be as strong as necessary while remaining light enough to save weight for space-based missions. Once optimized, the results are compared against each other as well as an "industry standard" quasi-isotropic tank made to be just strong enough under the same loading conditions. Cryogenic propellant tanks have been made in the past using CFRC, but this is an exploration into making the tank as well-made as possible. Doing this involves modeling the tank and optimizing it in Altair's design and simulation platform HyperWorks. As seen in figure 2.1, the tank is 1.9 meters in total length with a radius of 0.5 meters all around. To avoid the use of any proprietary information, the dimensions and geometry of the tank have been invented just for this computational investigation. The body consists of a cylinder 1.0 meter in length with two hemispherical domes of radius 0.5 meters on both ends. To account for the manufacturing process in which the tank is made on a lathe-like tool such as the one in figure 2.2, both of the domes have holes cut on the end whose diameter is 0.44 meters; approximately the average shoulder width of an adult. The holes are modelled to be filled with a thick steel plate for accurate static analysis when an internal pressure is applied. Without the steel plates, it would be as if some pressure is allowed to escape from the end-holes in the vessel. The tank is made to have similar dimensions as some seen in industry today and can also be scaled-up.

2.1 Model Creation

2.1.1 Geometry and Meshing

The model's geometry is made in Altair's HyperWorks 3D geometry tool, consisting of a cylinder and two hemispheres, all of which a hollow shell. After sectioning off the geometry

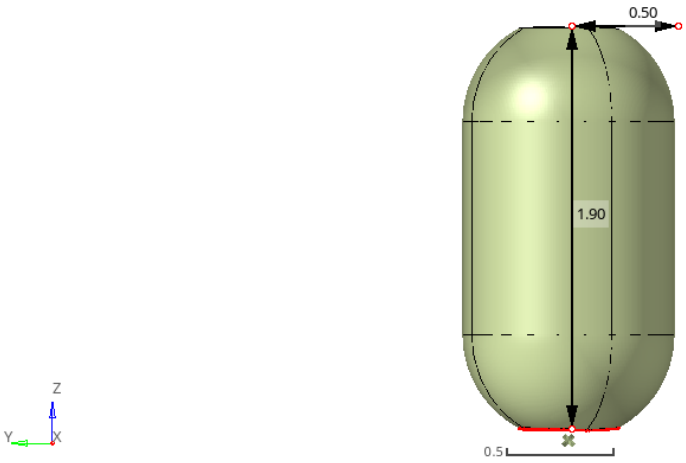

Figure 2.1: Design and dimensions of the propellant tank.

and making sure all of the surfaces are stitched together, a very fine 2D mesh consisting of over 65,000 elements is applied to the surface. The amount of elements in a mesh can be thought of as pixels on a screen; the more pixels (elements) there are, the higher resolution the image (results) will be. However, simply making the elements as small as HyperWorks will allow is not advisable. The program performs mathematical calculations at every element corner (node), so the computational cost needs to be taken into account to have just a fine enough mesh as is necessary to achieve desirable results. Next, circular holes are cut on each end using the cut holes tool and are filled with a surface and meshed as well.

2.1.2 Material Cards

Once the geometry is made, the Material Cards are made to be assigned to the tank. Within Hyperworks, a right-click within the model browser can be used to easily create most cards. First and foremost, a T700GC CFRC Material Card is made using a $MAT9OR$ image card. $MAT9OR$ image cards are used for composite materials in HyperWorks due to their anisotropy as discussed in section 1.2. The properties used to define the material are pulled from a study by the National Institute for Aviation Research (NIAR) looking at the material properties of Toray's T700GC CFRC [13]. The values used in this study are taken from specimens that were cured at room temperature since that is a very common curing method

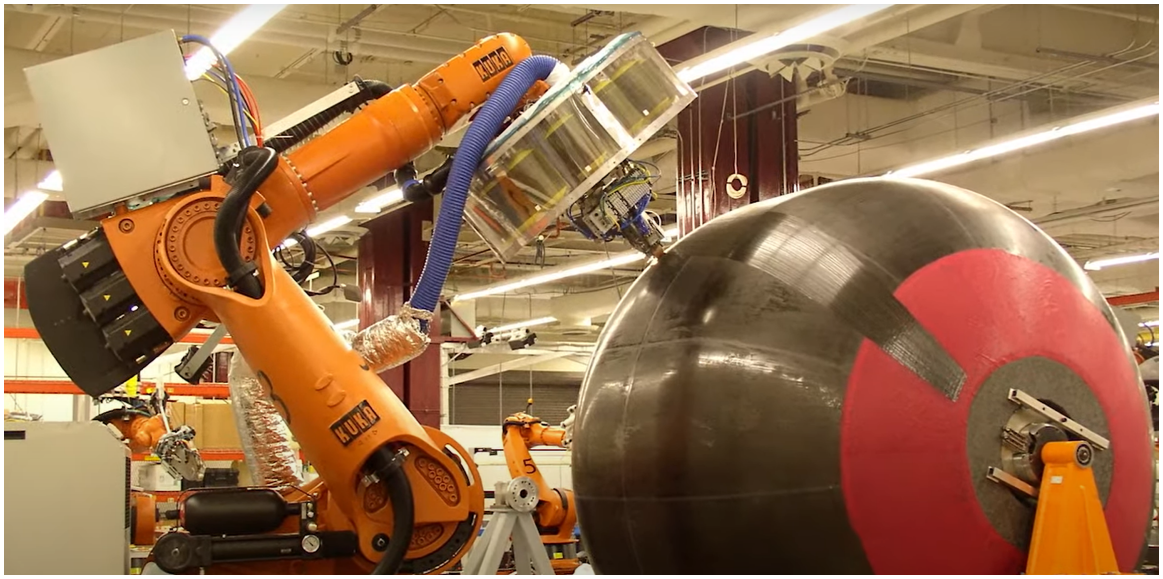

Figure 2.2: AFP-made tank being made on a lathe-like tool.

used for large CFRC structures. Values for material density (RHO) and Young's Modulus (E) in the 1 and 2 directions are all input in SI units (kg-m-s) to maintain consistency, where $E_3 = E_2$ as discussed in section 1.2. Values for the Poisson's Ratio (ν) in the 1-2 shear direction are also taken directly from NIAR, knowing $\nu_{12} = \nu_{23}$. However, using equation 1.6, ν_{31} is obtained knowing $\nu_{12} = \nu_{13}$. Values for the Shear Modulus (G) in the 1-2 shear direction are also taken directly from NIAR, knowing $G_{12} = G_{31}$. However, G_{23} is obtained using equation 1.4.

Temperature also plays a big role in the physical properties of a material, especially at incredibly low temperatures. The A-values in the Material Cards refer to the coefficients of thermal expansion in the 1, 2, and 3-directions. Values are pulled from class lectures using this same material, but similar values are also available on the TORAY website[14]. At the time of this thesis, the Hyperworks software optimizer does not obey the stress allowables when using Tsai-Wu failure criterion for $MAT9OR$ cards, thus leading to invalid results. One way around this is to use a $MAT8$ card for Tsai-Wu failure analysis, because the optimizer does obey the stress allowables in the two-dimensional case. The results are valid, but it is recommended to use a $MAT9OR$ card whenever possible. All values are input into

Card Image:	MAT9OR
User Comments:	Hide In Menu/Export
E1:	124823000000
E2:	8405000000
E3:	8405000000
NU12:	0.309
NU23:	0.309
NU31:	0.020806
RHO:	1525.0
G12:	4226000000.0
G23:	3210466005.0
G31:	4226000000.0
A1:	-5.39e-07
A2:	3.24e-05
A3:	3.24e-05

Card Image:	MAT8
User Comments:	Hide In Menu/Export
E1:	124823000000
E2:	8405000000
NU12:	0.309
G12:	4226000000.0
G1Z:	4226000000.0
G2Z:	3210466005.0
RHO:	1525.0
A1:	-5.39e-07
A2:	3.24e-05
TREF:	
Xt:	2167623000.0
Xc:	1447895000.0
Yt:	48857000.0
Yc:	198665000.0
S:	154740000.0

Figure 2.3: Material Card material properties input for Toray's T700GC with data from NIAR, all in SI units. On the left is the $MAT9OR$ card, the right is the $MAT8$ card.

the Material Card as shown in figure 2.3.

A $MAT1$ Material Card is also made for the isotropic steel hole coverings. These values are common values obtained from reputable sources [15].

Failure Criteria

Within the Material Card, the failure criterion needs to be defined so we can later analyze whether the pressure vessel can handle specific loading conditions. Two failure criteria are defined within the Material Card, a linear curve-fit criteria called Maximum Strain First Ply Failure and a quadratic curve-fit criteria called Tsai-Wu First Ply Failure. These are empirical curve-fit composite failure models which are limited because they are based on fitting within the bounds of available data rather than being proven physics-based failure models. That being said, with what is available now, empirical curve-fit composite models are commonly used in industry for composite design purposes [16]. It is worth noting here that this is done for the sake of performing the optimization of the structural behavior.

These empirical models cannot capture energetic and energetic-statistical size effects as well as progressive damage which are known to be important characteristics of composites [17, 18, 19, 20, 21, 22, 23, 24, 25, 26, 27, 28, 29, 30]. They also neglect the effects of crack parallel stress which was recently shown to diminish the equivalent fracture energy in composites [31]. Once the optimal structural configuration is identified, progressive damage computational models with embedded characteristic lengths can be used to predict the failure behavior more accurately. A number of computational models developed by the MAMS group at the University of Washington can be found in [32, 33, 34, 35, 36, 37, 38, 39, 40, 41].

The values for T700GC's failure criteria are taken from NIAR data, a very common database done by the National Institute for Aviation Research [13]. Tsai-Wu input values are stress-based and can be directly plugged into the five fields on the right side of figure 2.4. In the NIAR data sheet, the stress allowables are represented in the results using capital F. Max Strain are strain-based allowables are input into the nine fields on the left of figure 2.4. These values are obtained using the stress-strain relationship $\sigma = E\varepsilon$, being sure to use the correct E values with their respective σ's. Notice how some values such as V3 and V5 are the same. That is because V3 defines the tensile allowable strain in the 2-direction perpendicular to fiber direction and V5 defines the tensile allowable strain in the 3-direction which is also perpendicular to the fiber direction.

2.1.3 Material Property Cards

Next, a Material Property is made and assigned using a $PCOMPP$ image card which is commonly used when modelling composite laminate material. This is where we can define the Z_o offset, or the distance from the shell surface to the bottom of the first ply. Most often, $Z_o = -\frac{T}{2}$ is used where plies are stacked about the mid-plane, which is half the total laminate thickness as seen in figure 2.5. However, sometimes $Z_o = 0$ is used where the plies stack above the surface as if the plies are being layered on a table. Or least common, $Z_o = -T$ is used where plies are stacked below the surface, as if plies are being laid on the underside of a table. For this thesis, the default $\frac{-T}{2}$ is what is used. Within

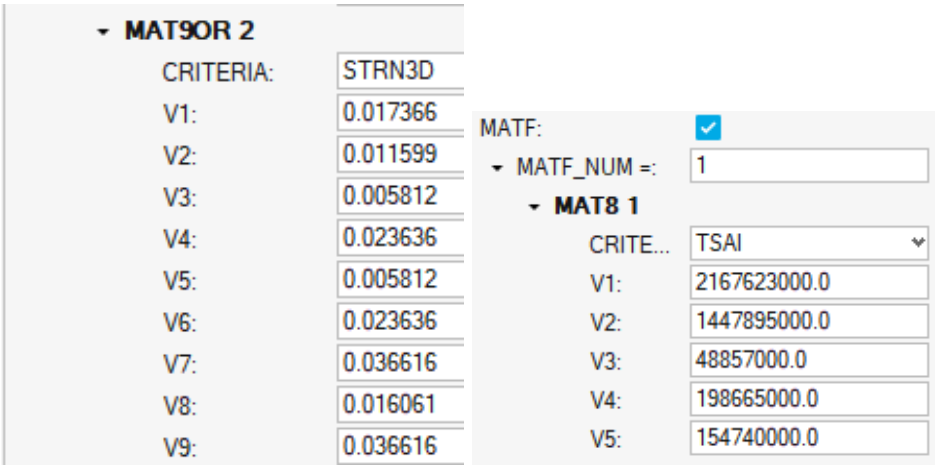

Figure 2.4: Material Card failure criteria input for Toray's T700GC with data from NIAR, all in SI units.

the Property Card, failure theory (FT) code can also be included, so it is recommended to make a Property Card for each failure theory intended to be used, such as Tsai-Wu and Max Strain. Care has to be taken to ensure the correct property is assigned to the model when doing different evaluations for different failure theories. So when optimizing by Tsai-Wu failure theory, the Tsai-Wu property card should be assigned for good practice.

Component Cards

The Material Cards and Property Cards are "assigned" to their respective components in a Component Card. This assigns which materials and properties go to which specific elements in the mesh. Otherwise, the model would be an empty geometry not made of any material.

2.1.4 Applying Loads and Boundary Conditions

When applying loads and boundary conditions, first a Load Collector must be created with no card image necessary. In the active boundary condition collector, a single-point constraint is assigned to the center of the bottom steel plate to hold the model in place, while the other end is left free to maintain a free-body. When the pressure Load Collector is active, an internal pressure of 0.375 MPa is applied to the entire model. To ensure the

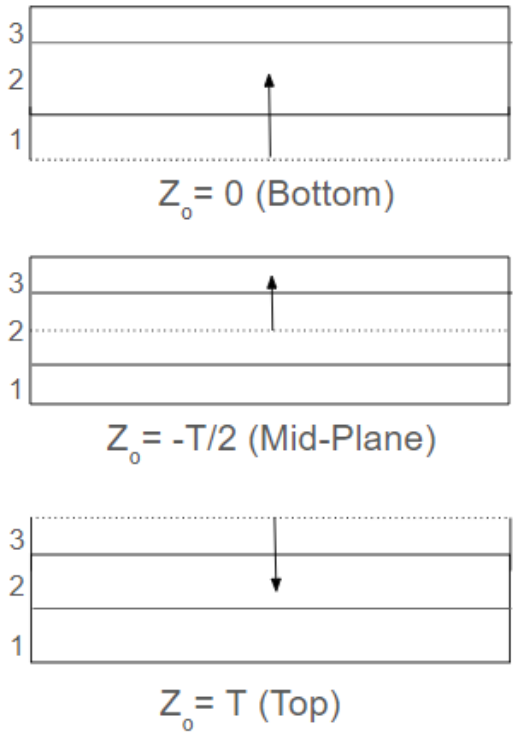

Figure 2.5: The three offsets for composite laminates, $Z_o = -\frac{T}{2}$ is the most common.

pressure is an internal pressure, the element normals can be checked. For space-bound cryogenic propellant tanks, the working pressure is typically around 0.2-0.3 MPa [2]. With a factor of safety (FOS) of 1.5, a pressure of 0.25 MPa becomes 0.375 MPa, higher than the high-range of pressures present in these type of propellant tanks.

Since the tank will hold fuel held at cryogenic temperatures, thermal effects come into effect. To account for this in the model, a Load Collector with a $TEMPD$ card image is made for the curing temperature assuming a common room-temperature cure for the CFRC of 20 °C. For the lowest temperature at which the model will reach, some assumptions are first made.

Loading Temperature

For the loading temperature, or the temperature at which the model will likely operate when in use, factors such as fuel temperature and insulation need to be taken into account. There

are a few different ways to insulate liquid hydrogen fuel (LH2) in a cryogenic propellant tank, ranging from foams to aerogel to even a vacuum between the walls. A vacuum between the walls is difficult to achieve and foams tend to require the tank to be larger than necessary because it takes up so much volume inside the tank. Aerogel tends to have limited mechanical properties, but it has an extremely low thermal conductivity, meaning it takes heat a long time to move through the aerogel material. Assuming a somewhat dense aerogel insulation layer (0.48 g/cm^3) that is 5 cm thick between the tank walls and the liner, the time to reach steady-state thermal conditions is four hours [42].

In the NASA Space Shuttle, the three main engines use LH2 with liquid oxygen oxidizer for their reusable rocket. Fuel tanks for rockets such as the one used by NASA in the 2020 Space-X Demo 2 launch are filled about 45 minutes before launch [43]. A total time-in-tank of about two hours is assumed to account for possible delays between fueling and launch. Thus, the assumed operating temperature of the tank with an aerogel insulation layer is taken to be half of the LH2 cryogenic temperature. So a Load Collector for the model temperature is made at -119.5 °C.

Load Step

The Load Step is where the solver and optimizer is told what is happening to the model at specific times. Multiple Load Steps can be created, but for this case, a single Load Step that happens instantaneously is all that is needed since we are not interested in how the model changes over time as it gets colder. Instead we only care about how it reacts as it is in its coldest state under pressure when the tank is completely full.

Within the Load Step, the Single Point Constraint (SPC) and the pressure ($LOAD$) is defined. Also, some Subcases can be defined within the loadstep. The $ANALYSIS$ Subcase is requested for a statics analysis and the temperature change is defined by requesting TEMP for the curing temperature and $TEMP\_LOAD$ for the loading temperature -119 °C. Some $CFAILURE$ (Composite Failure) is also requested within $OUTPUT$ as well as $CSTRAIN$ and $CSTRESS$.

2.1.5 Making the Composite

The only thing left to do to have a completely defined model is to actually make the model made out of carbon fiber reinforced composite (CFRFC). Up to this point, the model has been made as if it is a shell made out of carbon fiber. But in reality, the model is made out of many sheets of CFRC laid on top of one another in various orientations. The Composite Browser is where this can be defined.

First, a System Collector is made to define an axis it the base of the model, with the x-axis pointing along the length of the model. This is to define the 1-direction (0 °) along the length of the tank. Next, Plies can be created such as the one in figure 2.6. What needs to be defined is the ply thickness, orientation relative to the defined 1-direction, material, and shape. The shape refers to how the specific ply that is defined is shaped. Such as being the entire tank, just the walls, etc.

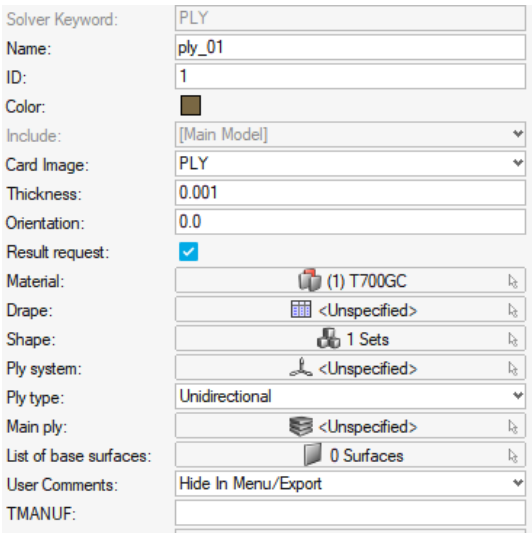

Figure 2.6: Example of a simply-defined Ply. TMANUF can also be defined to specify the thickness of a real individual ply of the chosen CFRC.

Once all the necessary plies are made, a Laminate is created and all of the plies can be placed into it. This can be thought of as the process of taking all of the individual plies and then stacking them on top of one another directly onto the model. Within the Laminate,

the Card Image is set to $STACK$ because the plies are stacked, and the Laminate Option is set to $SMEAR$.

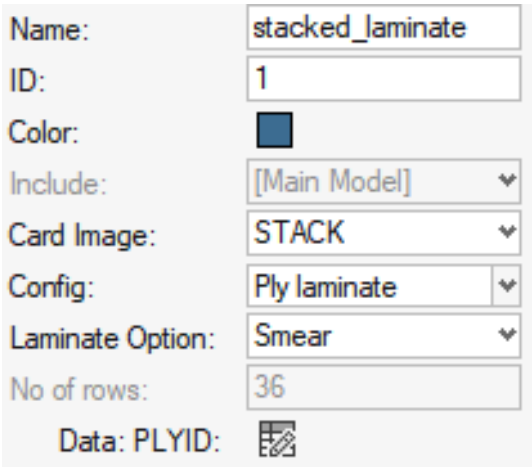

Figure 2.7: Example of a simply-defined stacked Laminate.

SMEAR

When optimizing composite-made models, the concept of $SMEAR$ and when to use it is one of the most important concepts to understand. In a nutshell, $SMEAR$ homogenizes the plies through the thickness of the stacked laminate when the stacking sequence of the laminate is initially unknown. This is done by utilizing the homogenous plate [B] and [D] matrix equations with the laminated plate [A] matrix [16]. To fully understand how $SMEAR$ works, we first must understand the [ABD] matrices, defined using Classical Lamination Theory as follows:

$$[A]_{lam} = \sum_{k=1}^{n} ([\overline{Q}]_k (z_k - z_{k-1})) \tag{2.1}$$

$$[B]_{lam} = \frac{1}{2} \sum_{k=1}^{n} ([\overline{Q}]_k (z_k^2 - z_{k-1}^2)) \tag{2.2}$$

$$[D]_{lam} = \frac{1}{3} \sum_{k=1}^{n} ([\overline{Q}]_k (z_k^3 - z_{k-1}^3)) \tag{2.3}$$

Where $[\overline{Q}]$ is the plane stress global stiffness matrix for the k^{th} ply and the z terms are the geometric distances from the stacked laminate mid-surface.

The [A] Matrix

In Classical Lamination Theory, the [A] matrix relates mid-surface strains to plate resultant forces which defines the extensional behavior of a laminate. This matrix is independent of stacking sequence for a laminated plate because the geometric terms from equation 2.1 $(z_k - z_{k-1})$ are always positive and equal to the thickness of the ply. Since the plies are always multiplied by their thicknesses regardless of their position in the stack, the [A] matrix is independent of the stacking sequence.

The [B] Matrix

In Classical Lamination Theory, the [B] matrix relates mid-surface curvatures to plate resultant forces and mid-surface strains to plate resultant moments which defines the coupling behavior of laminates. While the [B] matrix is stacking sequence dependent, notice from equation 2.2 that $(z_k^2 - z_{k-1}^2)$ are negative for negative z-coordinate plies and positive for positive z-coordinate plies. Additionally, the geometric terms are also symmetric about the middle surface, thus making the [B] matrix zero for symmetric laminates. Since we are ensuring a symmetric stacked laminate in this thesis, the stacking dependence of the [B] matrix goes away.

The [D] Matrix

In Classical Lamination Theory, the [D] matrix relates mid-surface curvature to plate resultant moments which defines the bending behavior of laminates. While the [D] matrix is stacking-sequence dependent, some notes can be made to made the [D] matrix independent of stacking sequence. Since 0°plies have the highest $\overline{Q_{11}}$ values, their location in the stacking sequence influences the bending behavior of the laminate greatly along the length of the fiber. The further away from the mid-surface the 0°ply is, the stiffer the laminate is in bending that direction. This is the same for 90°plies transverse to the fiber direction. If a

laminate is balanced and anti-symmetric, which we are ensuring, then the bending-twisting coupling of the laminate goes away. If all possible combinations of stacking sequences for a laminate are analyzed, the average [D] matrix $[D] = [A]\frac{T^2}{12}$ is equal to $[D]_{smear}$.

The final [ABD] matrices can be expressed as follows:

$$[A]_{smear} = \sum_{k=1}^{n}([\overline{Q}]_k(z_k - z_{k-1})) \tag{2.4}$$

$$[B]_{smear} = 0 \tag{2.5}$$

$$[D]_{smear} = [A]_{smear}\frac{T^2}{12} \tag{2.6}$$

$SMEAR$ is used in modeling composite materials when we do not know the final stacking sequence, which usually is not until the end of the optimization process. For this thesis, three optimizations are carried out. All three use $SMEAR$ technology and it is not turned off until a final linear static analysis is carried out where we know the final order of the plies in the laminate.

2.1.6 Global Output Request

Lastly, some outputs are requested using the Global Output Request and general Output cards. In the Global Output Request card, we can request to see results for $CFAILURE$ specifying an h3d format, $CSTRAIN$ specifying mechanical and thermal strain, $CSTRESS$, and $DISPLACEMENT$. This is all present in the output files for viewing in Hyperview after running the model. In the general Output card, we request a SZTOSH keyword which specifies a free-size to shape optimization output. This essentially says that the optimization has "free thickness" because we do not know how many layers of the CFRC we need yet, thickness refers to the amount of plies needed.

2.2 Linear Static Analysis and FEA

Before running any kind of optimization, it is good practice to check the model for any mistakes using a simple linear static analysis. Since the model is fully defined without any optimization inputs yet, a linear static analysis should run fairly quickly if made right, the order of a minute or two depending on how fine the mesh is. For this model, the mesh size

is approximately 70,000 elements which is somewhat of a fine mesh. How exactly the first model is stacked in the laminate comes up when discussing the first optimization, so long as there are plies in a stack that are fully defined, then a linear static analysis can be carried out by clicking $ANALYZE$.

An example of a linear static analysis run before any optimization is done can be seen in figure 2.8. Once opening the "s1" file in Hyperview, the final linear static results are available by looking at the contour map for the Y-Stresses on the last frame of the last iteration carried out by the solver. Y-Stress refers to stress in each element transverse to the defined fiber direction. More specifically, this is on the entire laminate scale, so it is referred to as the "hoop stress." On the scale of an individual ply, the Y-Stress would refer to matrix-direction stress, or σ_2. As well as composite stresses, outputs such as composite strains and failure criteria can be analyzed so long as they are defined and requested in output as discussed earlier. In figure 2.8, note that the stress is on the order of a few MPa, and the geometry is not distorted. These both indicate we are in the ballpark of a reasonably defined model and can move on to optimization.

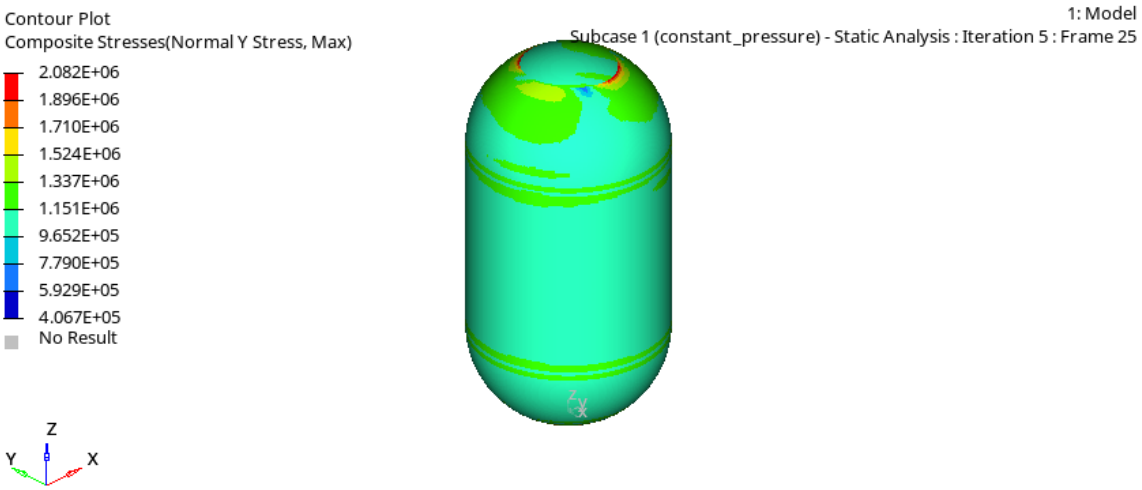

Figure 2.8: Example output of a linear static analysis run before any optimization was done on the tank. Y-Stress refers to the stress in each element transverse to the fiber direction [Pa], or the Hoop Stress since this particular output is on the laminate scale. This would be the matrix-direction stress, σ_2, if this was on the scale of a single ply.

2.3 Optimization

Optimization of a structure is the design process in which you take an initial design and try to make it as "good" as possible according to set goals and restrictions put in place. Often, such as in this thesis, the goal may be to reduce mass while still being able to withstand certain initial and boundary conditions. In this case, the goal is to reduce the mass of the tank as a free body while being able to withstand an internal pressure of 0.25 MPa (0.375 MPa after a factor of safety of 1.5 is applied) and a total temperature difference of 139.5 °C.

Mathematically, optimization is the minimization of the objective function $f(X) = f(X_1, X_2, X_3, ..., X_n)$ subject to constraint functions $g_j(X) \leq 0$ from $j = 1, ..., m$ design constraints for design variables X_i which can have upper bound limits $X_i^L \leq X_i \leq X_i^U$ from $i = 1, ..., n$ design variables [16]. Design variables are physical properties that can be changed within a model, such as the thickness of the model which leads to the amount of plies used. The objective function is the goal of the optimization, in this case minimizing mass. The constraint functions are responses that must be satisfied, such as allowable stress in the direction of the fiber. In this optimization problem, the objective is to minimize the mass of the model.

Since the mathematical objective is finding the minimum of a function, $f(X)$, the idea can be generally expressed graphically. In figure 2.9, the objective function is represented as a line on the graph with various minima and maxima that stretch infinitely in either direction. In optimization, the ultimate goal is to reach the lowest point, or global minimum. The red dot represents the initial conditions such as an initial thickness design variable we feed the optimizer. The optimizer then goes through multiple iterations lowering the mass until the design constraints are no longer satisfied, after which it falls back to the lowest mass iteration that still fell on the graph that it passed, represented by the blue dot. But the optimizer will not go over maxima through iterations, meaning the red dot will only fall down, not go back up the hill to the right of it. So how do we get to the global minimum, represented by the purple dot? To overcome this, we can change the initial conditions we feed the optimizer to shift the red dot to the other side of the hill, so it falls towards the purple

dot instead, such as a different initial thickness. We can never know with 100% certainty that our optimization has reached a true global minimum, but we can reach reasonable conclusions by changing the initial conditions and re-running the optimizer. By optimizing with new initial conditions far to the right and left of the suspected global minimum initial conditions, we can see if we get the same mass or not. If we keep getting the same mass or a higher mass, we can conclude with some certainty a global minimum has been reached.

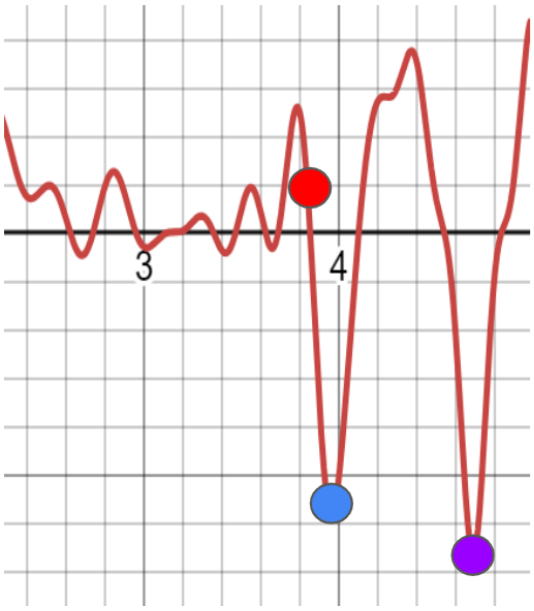

Figure 2.9: Graphical representation of optimization. Red represents the initial conditions fed to the optimizer, blue represents a local minimum, and purple represents a global minimum.

A common way to define the problem for optimization is to go through the **DRCO**s of the problem. Each optimization run explicitly states the **DRCO**s.

Design Variables Things that can change in the model, such as thickness.

Responses Values measured from model changes, such as allowable stress.

Constraints Limits on responses of the model that must be satisfied.

Objectives Single response of the model to be minimized or maximized, such as the mass.

For composite design optimization, the problem starts out as a broad one and slowly gets restricted more and more. The most broad representation of the model and how the plies are constructed comes first and the optimization gets broken into smaller, simpler optimizations.

2.4 Optimization 1: Optimizing the Angles

The first optimization is interested in what ply orientations perform the best under the conditions we are placing the model. Plies in a composite structure can vary from $0° - \pm 90°$. There are some commonly used ply orientations for specific reasons in a pressure vessel visualized in figure 2.10. Hoop winding is often paired with low-angle helical winding to prevent fibers from separating in one direction. Since carbon fiber reinforced composite is strongest along the length of the fibers, if the tank was made entirely of hoops, then the tank would split apart along the dotted line. The low-angle helical plies help hold the tank together along the length. Also, having helical layers that mirror one another (such as +45°and -45°) is what makes the composite structure symmetric. This helps with shearing effects because as the positive helical layer helps off-axis stress in one direction, the negative helical layer helps with the opposite off-axis stress in the other direction.

Since the goal of optimization is starting with a broad problem and narrowing it down using smaller and smaller ones, this first optimization takes the pressure vessel and includes layers all in the same thickness ranging from $0° - \pm 90°$ in 5°increments taking up the entire model shape. This way all the orientations can be analyzed by looking at which ones are the thinnest in the "_des" output file loaded into Hyperview. Going to the final frame of the last iteration, the orientation thicknesses can be individually looked at. The thinner orientation layers mean they are the ones that can handle the applied conditions most efficiently.

To do this, in the Optimize tab, the Design Variable $DSIZE$ card is applied to the stacked laminate and made to be a free-size $CONFIG$, meaning it is a free-size optimization. The $MINDIM$ is set to eliminate really small members in the optimization. For this model, 0.1 m is used as the smallest dimension allowable. Here is also where $BALANCE$ is set

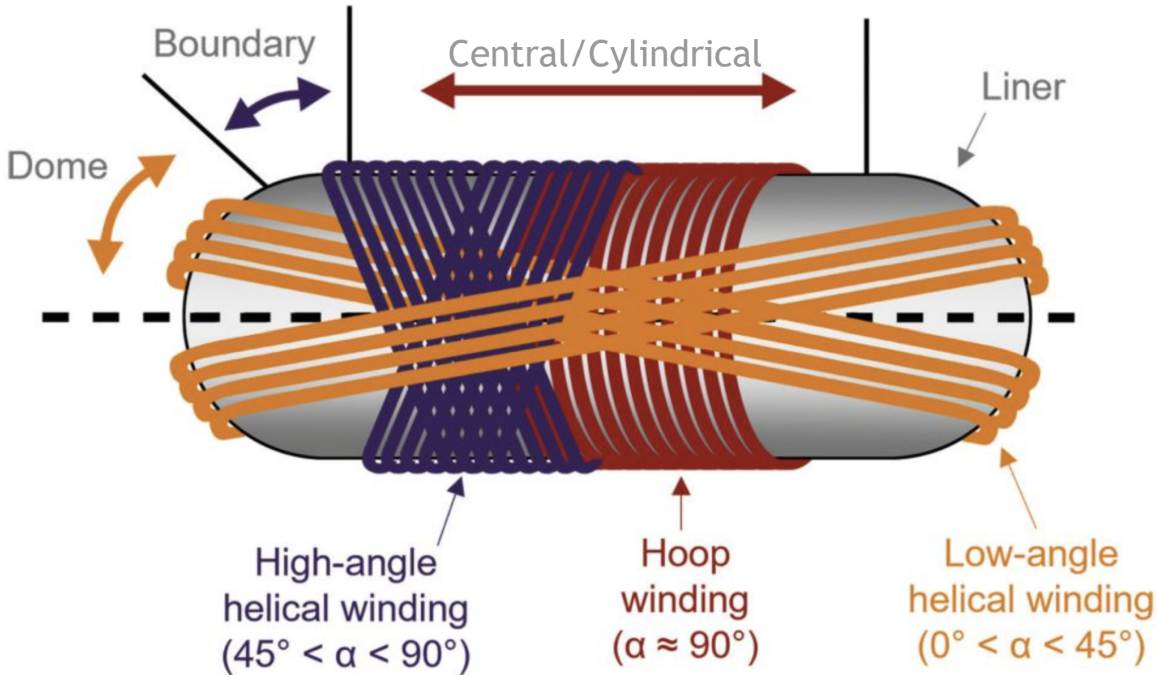

Figure 2.10: Classes of tow windings on a cylindrical vessel made of CFRC. Courtesy of Jeff Wollschlager.

using a table entry, ensuring all positive angles on the left-hand side of the table have their corresponding negative angles on the right-hand side of the table. This tells the optimizer that every positive angle thickness must have its negative angle match in thickness to maintain composite balance. The only orientations that do not need to be in the table are the 0°and 90°plies because $+90° = -90°$ and $+0° = -0°$.

Next, the Responses $DRESP1$ cards need to be made. The two responses are the volume fraction and the compliance. For the volume fraction response type, we will be soon telling the model to get the volume fraction to below a certain threshold to help us sort out which plies are most efficient. The compliance response type has to do with a measure of the susceptibility of the tank to deform due to the pressure and will be included in the objective.

The Constraint $DCONSTR$ is placed upon the volume fraction and is set to 0.3, telling the optimizer to get rid of all but 30% of the volume in the original model.

The Objective $DESOBJ$ is placed upon the compliance, giving the optimizer the objective type to minimize the compliance. By minimizing compliance, the structure is deformed the least.

2.5 Optimization 2: Optimizing the Shapes

Once the first optimization is done and the plies are known, next comes optimizing the shapes in which to have each orientation. This is set up the same way as the first optimization. However, now the balance table is changed to only include the plies that are decided to be used, and the initial thicknesses are increased to give the optimizer a thick laminate to work down from.

When looking at the output, the same _des output file is imported into Hyperview and the orientation thicknesses can be individually looked at again. Then ideas can be drawn from how the orientations may make the most sense in certain shapes, such as having 90°plies take up only the cylindrical walls.

2.6 Optimization 3: Optimizing the Numbers of Layers

Once the plies and shapes are known, these can all be put together into the "Shuffling Optimization," or the optimization in which the number of layers for each orientation in their assigned shapes is decided. By now, the ply orientations and their shapes have been fully defined in the stack, but we must whittle the model down to the minimum thickness necessary to meet design constraints.

For the Design Variables, the $DCOMP$ card is changed to a composite size optimization specifying the stacked laminate. Balance is applied to any helical layers. Now, Design Variables need to be made for each ply orientation, including the negative ply orientations. These are done by making a $DESVAR$ card for each orientation in which the initial value (the thickness of the individual ply in the stacked laminate) is given along with the minimum thickness (the thickness of a single ply, in this model's case 0.15 mm) and an upper bound. For the upper bound, it is recommended to just put it fairly high so the model is not accidentally over-constrained.

Now, the $DESVARS$ need to actually be assigned to their respective plies. This is done

using a Design Variable Relation called a $DVPREL$ card. For each ply, a $DVPREL$ is made to connect the ply to its $DESVAR$.

For the Responses and Constraints, now the optimizer will look to minimize mass based on the composite failure criteria we assign. Three failure criteria are used, each needing its own Responses and Constraints.

Note, for the Objective, the same objective is used no matter the failure criteria — minimize mass.

2.6.1 Stress-Based Failure Criteria Responses and Constraints

For Stress-Based Failure Criteria, the same allowable stresses as Tsai-Wu Failure Criteria are used since they are both stress-based models. This does not create a failure index, but instead looks at the stress in each element in each direction and optimizes to make sure the experienced stresses are below the allowables. This criterion is especially helpful since it can be done using the $MAT9OR$ material whereas the Tsai-Wu criteria can only use the $MAT8$ criteria. So we can look at stress criteria in the three-dimensional and two-dimensional case to cross-reference. Ensuring the $MAT9OR$ material is assigned in the component and as the material for each ply, the Responses and Constraints can be defined.

For the Responses, $DRESP1$ cards are made for the mass response type as well as for all of the stress allowables in tension and compression, as defined like the Tsai-Wu stress allowables. These have the composite stress response type where the property is defined as well as the direction such as, "normal 1," meaning along the 1-direction. Notice how the normal 3 is not requested but all three shearing directions are. That is because the normal 3 direction is the same as the normal 2 direction, but there are variances in the shearing allowable stresses. In this case, the 12 shearing is equal to the 1Z shearing, but not the 2Z shearing, the same as in Tsai-Wu.

For the Constraints, $DCONSTR$ cards are made for each allowable stress defined in the Responses. For each Constraint, the Load Step must be defined as well as the upper bound, which is the allowable stress. If an allowable stress is negative, take the absolute value and still set is as an upper bound.

2.6.2 Tsai-Wu Failure Criteria Responses and Constraints

For the Tsai-Wu Failure Criteria at the time of this thesis, as mentioned before a $MAT8$ material card has to be used. Care must be taken to be sure that the material is applied to the component as well as each ply. It should be noted here that this problem can be worked around by using what is called a $DREF2$ card to code in the correct three-dimensional Tsai-Wu failure equations. For this thesis, we ran out of time and as will be seen in the results, they match up well with the stress-based criteria.

For the Responses, only two $DRESP1$ cards need to be made since the Tsai-Wu failure criteria has already been defined as is embedded in the Hyperworks code. One for the mass as defined above, and one for composite failure response type. Below the region identifier is where Tsai-Wu can be defined. For the maximum amount of information we also requested output for each ply on the top and bottom.

For the Constraint, a $DCONSTR$ card is made for the cfailure Response at the Load Step with an upper bound of 0.99. Being a failure index, so long as the output is between $0 < x < 0.999...$ then the structure is deemed safe. A lower bound can also be defined to ensure the index is above 0 or a negative number.

2.6.3 Max Strain Failure Criteria Responses and Constraints

For Max Strain Failure Criteria, the material can be defined as $MAT9OR$ just like the stress-based criteria. Care must be taken to make sure the property assigned is the property made with the FT set to max strain. It is not entirely necessary since we are requesting all the failure indices as output anyways, but it is good practice.

For the Responses, the same $DRESP1$ Responses are used as in Tsai-Wu, only now below the region identifier max strain is defined.

For the Constraint, the same $DCONSTR$ card is defined as Tsai-Wu. Since this is also a failure index, the bounds are set to ensure the optimizer obeys the failure index criteria.

Chapter 3

RESULTS AND DISCUSSION

3.1 Optimization 1: Optimizing the Angles

The first optimization has the optimizer cycle through each ply from $0° - \pm 90°$ in $5°$increments. Once complete, the thicknesses of each orientation are analyzed and compared to look for trends. In general, between $0° - \pm 30°$, the walls are thin and get thicker and the dome is thick and gets thinner. From $\pm 30° - \pm 45°$, the total thickness increases and continues from $\pm 45° - 90°$.

Traditionally, $0°$plies tend to be the strongest except where constrained, which in the case of a cryotank will be on the ends when mounted. These $0°$plies are traditionally not placed on the dome ends. $90°$plies are traditionally placed only in hoop layers because when manufacturing, exact $90°$plies can raise a lot of manufacturing issues due to just how long they take compared to other orientations. Even a slight misfeed from the strands being laid by the robot makes the whole process stop, which is more possible as manufacturing time increases. In the world of manufacturing, this is often accounted for by making very high-angle "helictical" layers of $88°$or so instead of $90°$. Making the plies slightly helical also reduces any interference the robot may have with the spindles the manufacturing tool is mounted on. The tool is what the cryotank is made on which would be attached to the ends where the steel plates are modeled. Helical plies from $0° - \pm 90°$ traditionally make up the majority of the tank and are made from end to end. This is because they can be made quickly using AFP and also resist shearing forces well due to being at an angle. In the world of composite structure manufacturing, $0°$and $90°$plies will always be used, or at least one, due to their strengths along and transverse to the length of the structure.

Upon comparison and keeping traditional manufacturing methods in mind, four distinct ply orientations are chosen as seen in figure 3.1. These are viewed as what could be the highest-performing ply orientations. The $0°$and $90°$layers are chosen due to their strengths

along and transverse to the length of the cryotank. For the helical layers, $\pm 45^\circ$ is chosen for its traditional use and potential high performance against shearing, along with quick manufacturing time. What is fairly new and not as deeply explored yet are considered more "intermediate" helical layers such as $\pm 30^\circ$ plies. Because of this and the potential higher performance suggested by its total thickness being mostly less than $\pm 45^\circ$ all-around, $\pm 30^\circ$ is also chosen to be explored.

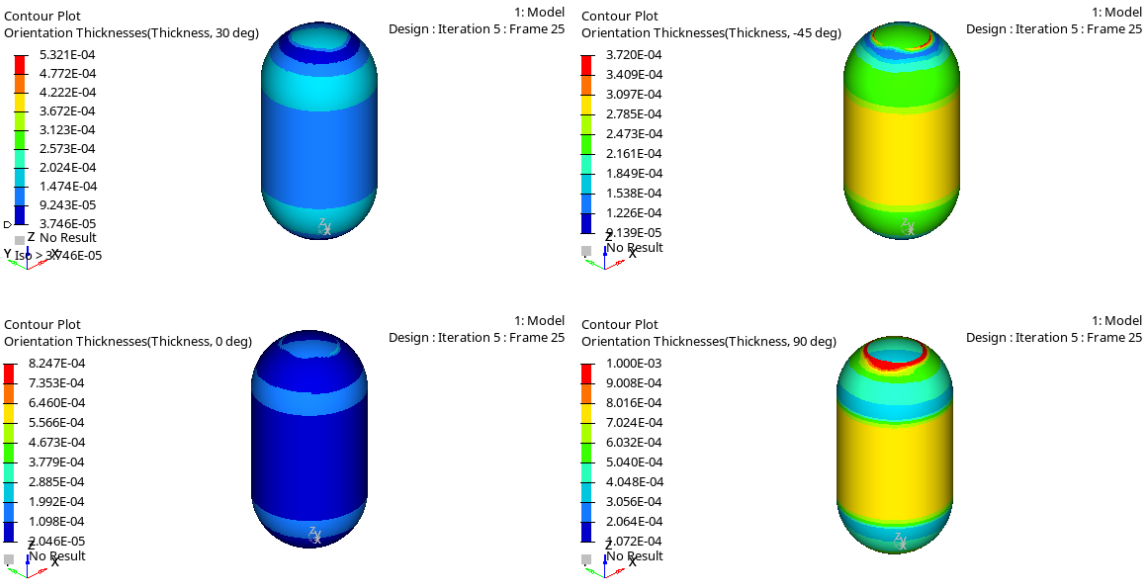

Figure 3.1: The four decided layers to be explored from the first optimization—$\pm 30^\circ, \pm 45^\circ, 0^\circ$, and 90°.

Also, the total thickness of the composite can be useful for understanding potential weight and time-saving techniques to use at an early stage. Noticeably, in figure 3.2, we see a thick cylinder wall with thinner spherical domes. This tells us that constant thickness is not necessarily needed since we can expect the spherical domes to transfer pressures more efficiently than the cylindrical walls. While the thicknesses are in units of [m], it should be noted that these are arbitrary thicknesses assigned at the beginning of the optimization, true thicknesses are not until the very end of the optimization process.

With the information gathered and plies chosen, these can be applied to the second

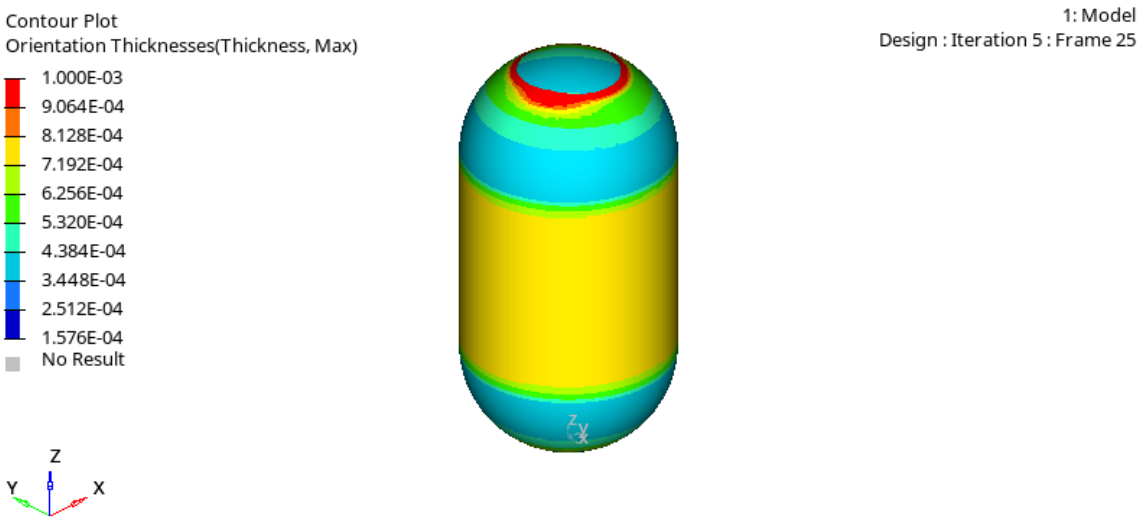

Figure 3.2: The total composite thickness after the first optimization. Units in [m] but the thickness for this optimization is arbitrary.

optimization to then understand possible shapes of the orientations.

3.2 Optimization 2: Optimizing the Shapes

The second optimization is simply the same as the first optimization but now with only the chosen plies, $\pm 30°, 0°$, and $90°$. The $45°$ply is not included in the shape optimization because that is going to be used as a comparison model to be discussed due to its traditional use as the helical layers for composite structures. The same output as the first optimization, the orientation thicknesses, is analyzed but now the focus is on the shapes of these orientations as opposed to their thicknesses compared to one another.

As mentioned before, $90°$plies are traditionally made on the cylinder walls only. If wanted to be used on the entire tank, $90°$plies are transformed into $88°$plies or so when being manufactured due to their performance being almost identical. However, this is not necessary to change when modeling. $0°$plies are traditionally not placed on the dome ends due to the robot not physically being able to lay that ply orientation so close to the spindles on the tool the tank is made on. Helical layers tend to make up the bulk of the tank due

to their ability to be made quickly and to oppose shearing forces the best, especially in the tank walls.

Inspecting the orientation thicknesses, a novel idea is introduced as a potential weight and time-saving technique. As seen in figure 3.3, the 0°ply is thinnest in the walls, as is expected. This means that the 0°plies are most efficient in the walls. However, there is a light blue band in the dome that is only slightly thicker than the expected thickness, or thinness, of the 0°ply at the walls. The introduction of 0°plies in the dome is proposed in contrast to traditional design techniques to explore the potential weight and time-savings. This area will be named the "0°Band." Also, as expected the ±30° ply is relatively thin all around the cryotank and will make up the main body of the novel approach. Lastly, the 90°plies are the thickest at the walls as expected, and will be used in the traditional method of keeping them at the walls.

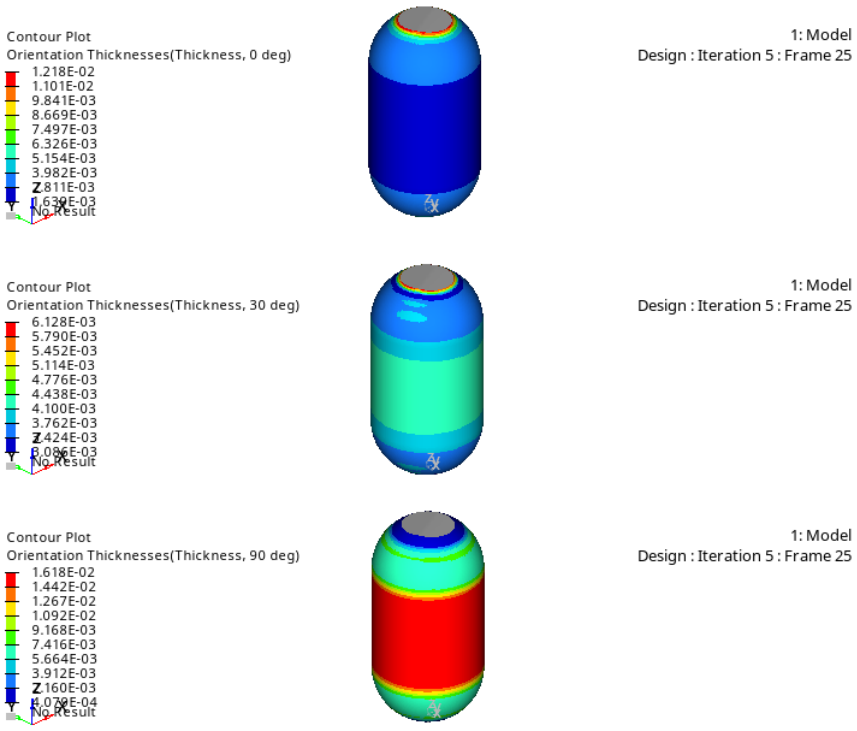

Figure 3.3: Orientation thicknesses after the second optimization. Also in units of [m] but still arbitrarily assigned thicknesses.

From the second optimization, a novel approach will be explored consisting of plies in the $0°, \pm 30°$, and $90°$directions. This approach will also be compared to what will be named the Traditional Tank, consisting of only $\pm 30°$ and $90°$plies. This is the same as the $0°$Band idea but with the $0°$band removed. Also, a Quasi-Isotropic tank, consisting of $0°, \pm 45°$, and $90°$plies all over will be used as the most traditional approach. The plies in the Quasi-Isotropic tank will all take up the entire shape of the cryotank. It is called Quasi-Isotropic because the lamina are oriented to make an isotropic [A] matrix, where $A_{14} = A_{24} = 0$, thus eliminating extension-shear coupling [44]. A summary of the three designs are shown below:

1. **Novel $0°$-Band Approach:** $0°$Band, $\pm 30°$ entire tank, $90°$in the walls.

2. **Traditional Approach:** $\pm 30°$ entire tank, $90°$in the walls.

3. **Quasi-Isotropic Approach:** $0°$, $\pm 45°$, and $90°$entire tank for every orientation.

The final ply shapes are made from the results of this optimization. The "full" shape takes up the entire tank except for the steel plate ends. The "wall" shape takes up the cylindrical walls, which are 1.0m in length. Both of these shapes are seen in figure 3.4.

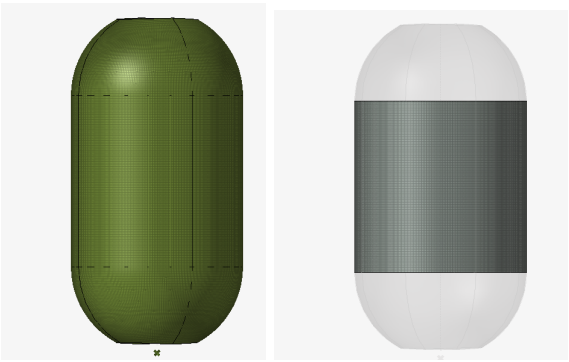

Figure 3.4: "Full" and "wall" shapes made as a result of the second optimization to be used in the third optimization.

For the $0°$-Band idea, the bands start at the intersection between the dome ends and walls as well as just before the end of the dome, seen on the far left of figure 3.5. An artificial

Figure 3.5: 0°-band shapes, from left to right is the 0_1, 0_2, 0_3, 0_4, 0_5 bands.

ply drop is induced by making shapes that taper in from both ends. To decide how much to taper, the grade of the ply drop should follow a ratio of $\frac{t}{L} = \frac{1}{20}$, where t is the total thickness and L is the length of the longest band. In this case, $L = 0.38m$ so that comes out to $t = 0.019m$. Using an individual ply thickness of 0.001m, this means in this length we can use about 20 plies and have a fine ply drop grade. Since I am using 5 shapes, each shape could be assigned an initial thickness of 4 plies and still be fine. However, all that is needed is a thickness of 2 plies per shape. The shapes are made by hand in Hyperworks by selecting elements. Each shape is tapered in about 4cm on either side on both ends of the dome from left to right as seen in figure 3.5.

3.3 Optimization 3: Optimizing the Numbers of Layers

The third optimization step is a total of nine optimizations. For each design approach, the three failure criteria defined before are used in each case to have layups made based on their respective allowables. First, the optimizer figures out how much of each ply is needed in the shapes given. This is analyzed in the "_shuffling.fem" output file. Then the plies are reordered for balance and symmetry, copying as few plies as necessary. In the same file, the **DRCO**s are deleted and rerun for a final linear static analysis.

3.3.1 The Novel 0°-Band Approach

Before reordering the plies, first the axial and hoop stresses can be analyzed to ensure the resultant stresses are within the allowable maximum stresses. As seen on the top half of

figure 3.6, for each criterion the maximum axial stress is at the walls of the tank. The differing stresses are due to the different criteria having different resultant layups after the optimization, especially seen in the Stress-Based Criteria compared to the others. These differences are expected because in general, the more layers present in the laminate stack the less resultant stress. The same is true in the hoop direction, as seen on the bottom half of figure 3.6. The hoop stress also falls within the maximum allowable hoop stress, verifying that the optimization was done correctly.

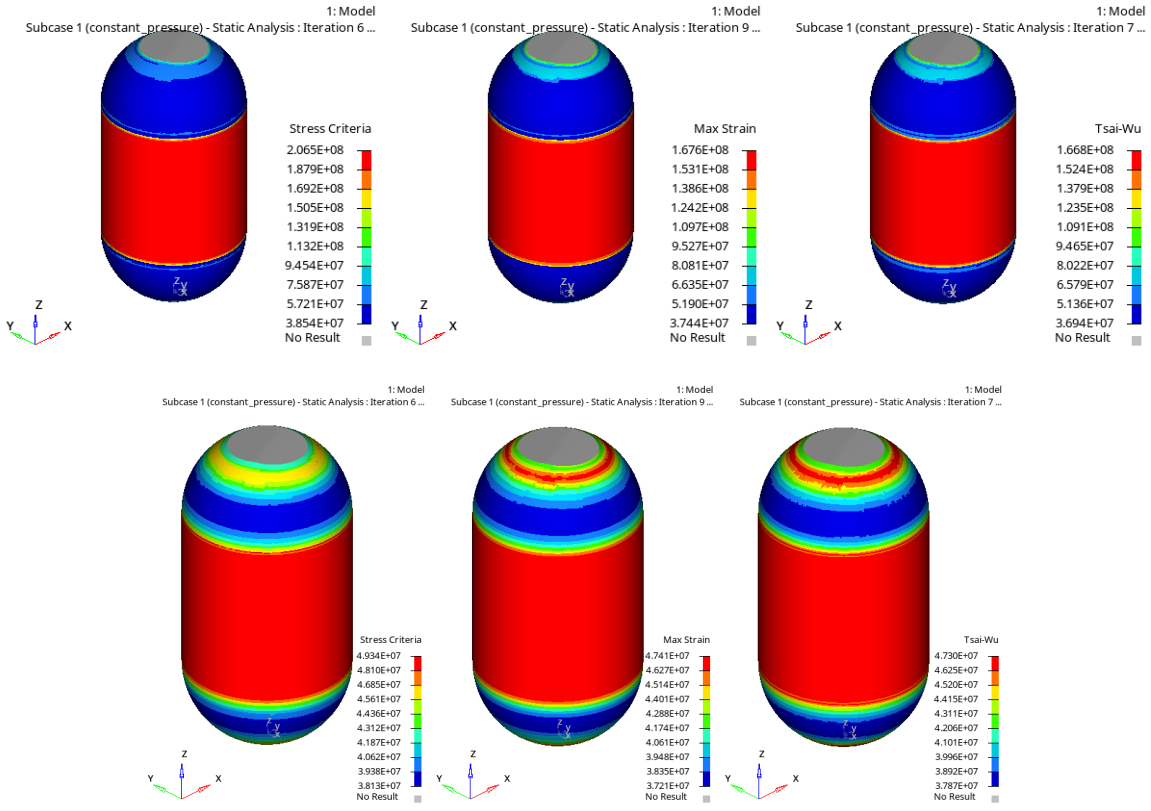

Figure 3.6: Axial stress on top and hoop stress on bottom for the 0°-Band Approach [Pa], before balancing the laminate stack.

Once the optimization is verified to have been done correctly, the final stacks can be made for each failure criterion as seen in figure 3.7. For Stress-Based Criteria, the optimizer recommends six plies each of ±30°, four 90°plies, and two of each 0-band ply, except for the

largest 0_1 band which has four. For Max Strain Criteria, the optimizer recommends the same amount of plies, except an extra two 0_1 plies. For Tsai-Wu Criteria, the optimizer recommends the exact same plies as using Stress-Based Criteria.

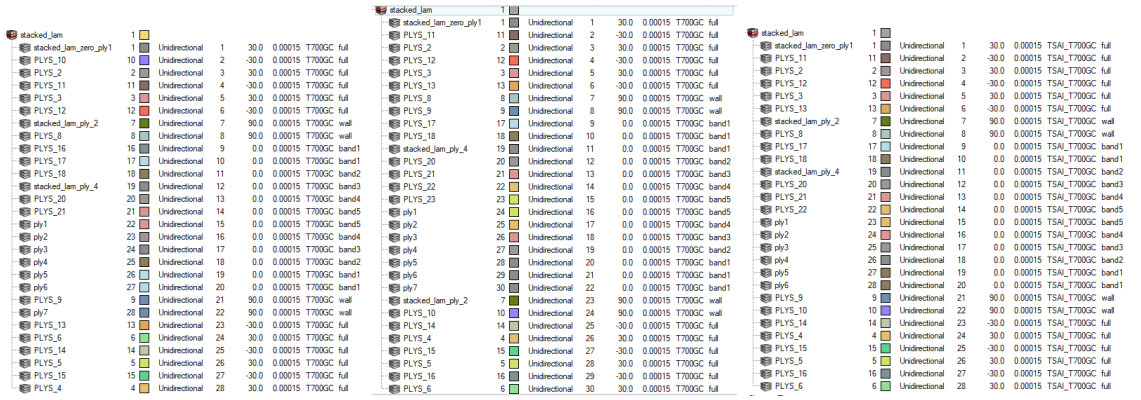

Figure 3.7: Final stack layup for the 0°-Band Approach. From left to right is the Stress-Based Criterion (28 total plies) $[(\pm 30)_3, 90_2, 0\_1_2, 0\_2, 0\_3, 0\_4, 0\_5]_s$, Max Strain Criterion (30 total plies) $[(\pm 30)_3, 90_2, 0\_1_3, 0\_2, 0\_3, 0\_4, 0\_5]_s$, and Tsai-Wu (28 total plies) $[(\pm 30)_3, 90_2, 0\_1_2, 0\_2, 0\_3, 0\_4, 0\_5]_s$.

The layup codes (seen in the square brackets in 3.7, are a short-hand way to write out the stacking sequence of a stacked laminate. The plies are layered top-to-bottom as they are read from left-to-right. If there is a $\pm$ sign, that means the plies are oriented with a positive orientation and a negative one. If there is an s outside the square brackets, that means the laminate is symmetric and the layers are all repeated from right-to-left to maintain symmetry. If the last number has an overbar (i.e. $\overline{90}$), that means the stacked laminate is symmetric about that particular ply, so do not repeat that ply. Lastly, if there is a number outside the square brackets or outside a ply within the square brackets, it means the stacking sequence is repeated that many times. For example,

$$[0, 45, -45, 90]_{4s} = [0, 45, -45, 90, 90, -45, 45, 0, 0, 45, -45, 90, 90, -45, 45, 0] \tag{3.1}$$

or

$$[(\pm 45)_2] = [45, -45, 45, -45] \tag{3.2}$$

For the 0°-Band approach, each failure criterion calls for almost the exact same layup. For Stress-Based criteria, the total output mass is about 23.4 kg, as is the mass for Tsai-Wu. For Max Strain, the total mass is about 24.5 kg. Looking at the resultant stresses, the maximum axial stress, that is the stress along the fiber direction for the stacked laminate, is about 168 MPa to 169 MPa as seen at the top of figure 3.8, well within the allowable axial stress by a factor of ~ 10. The minimum stress in the axial direction occurs at the domes, $\sim 37-38$ MPa. This is expected geometrically and also because the dome is reinforced. The resultant maximum hoop stress are all ~ 47.5 MPa seen at the bottom of figure 3.8, which is just below the maximum allowable hoop stress. This confirms that the main limiting strength factor will be the strength transverse to the fiber direction, which relies only on the strength of the matrix being pulled apart.

The failure indices for the final layups can also be analyzed respective to their own failure criterion as seen in figure 3.9. The areas closest to critical failure, a index value ≥ 1, are the cylindrical walls and near the ends of the domes where the steel plates are. This is also expected since the cylindrical walls are less efficient at distributing stresses compared to the domes, so critical failure is most expected at the walls or near the hole in the domes since that introduces an area of weakness.

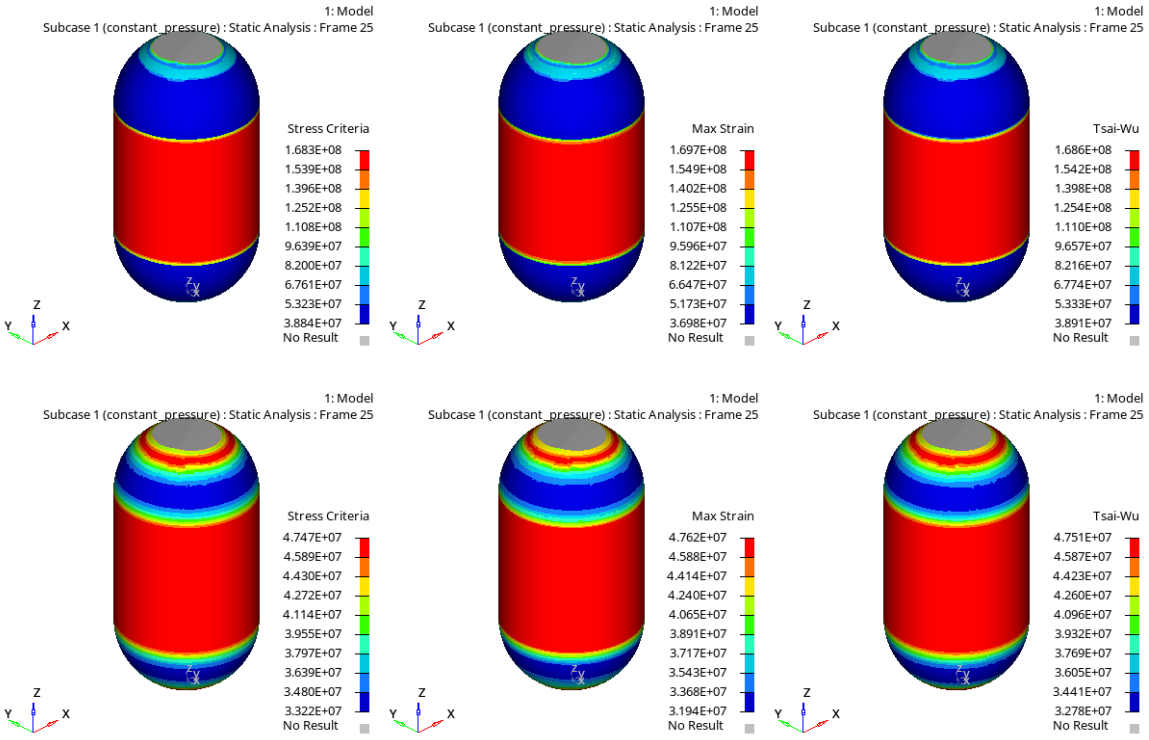

Figure 3.8: Final axial stress on top and final hoop stress on bottom for the 0°-Band idea [Pa].

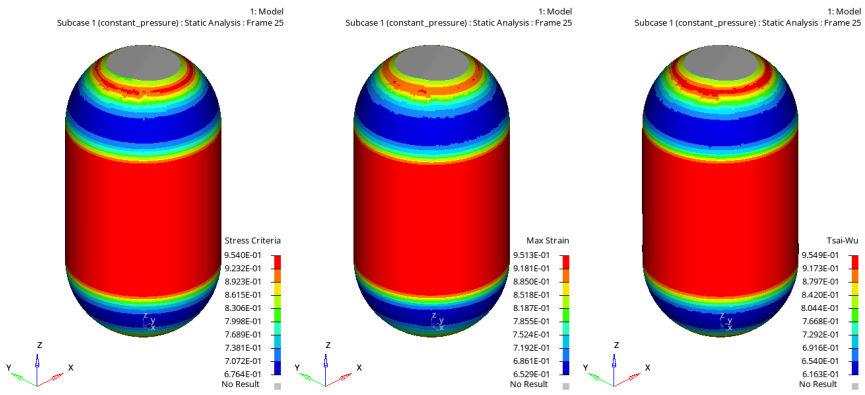

Figure 3.9: Final failure indices for the 0°-Band idea for all three failure criteria used.

3.3.2 The Traditional Approach

Before reordering the plies, the axial and hoop stresses can be analyzed to ensure the resultant stresses are within the allowable maximum stresses. As seen on the top half of figure 3.10, for each criterion the maximum axial stress is at the walls of the tank as with the 0°-band. The same is true in the hoop direction, as seen at the bottom half of figure 3.10. The hoop stress also falls within the maximum allowable hoop stress, verifying that the optimization was done correctly.

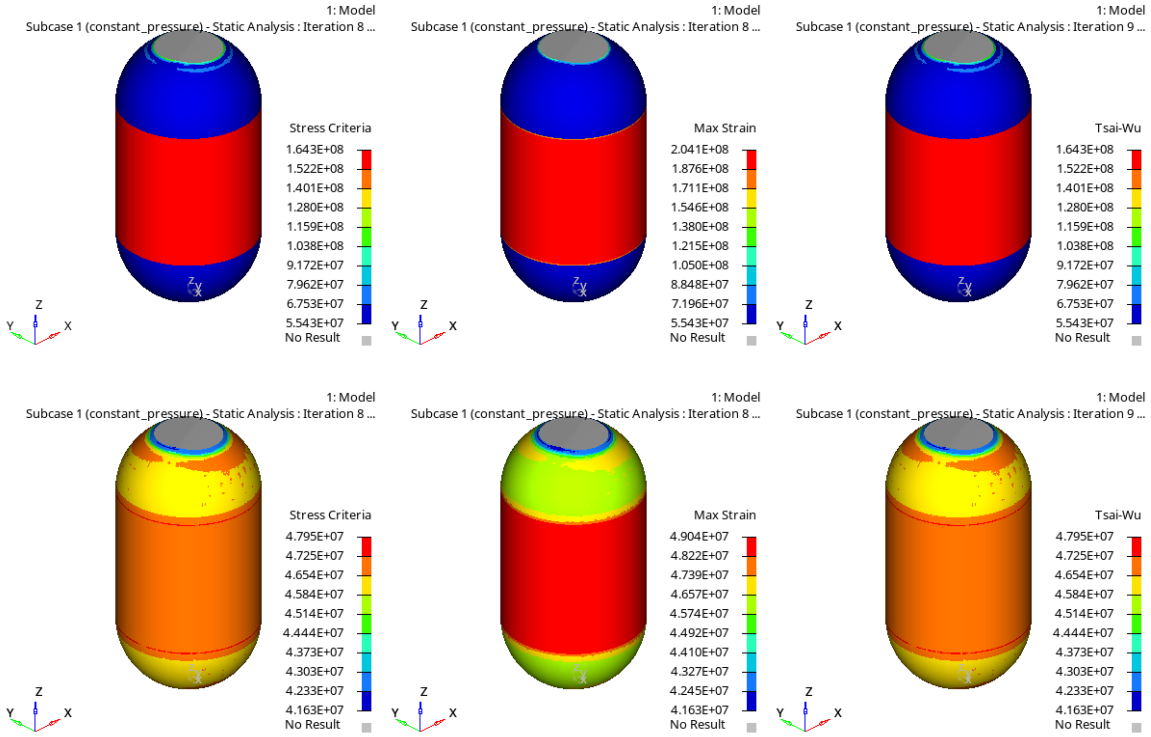

Figure 3.10: Axial stress for the Traditional Approach on top and hoop stress for the Traditional Approach on the bottom [Pa], before balancing the laminate stack.

Once the optimization is verified to have been done correctly, the final stacks can be made for each failure criterion as seen in figure 3.11. For Stress-Based Criteria, the optimizer recommends six plies each of $\pm 30°$ and four 90°plies. For Max Strain Criteria, the optimizer recommends the same amount of plies, except one less 90°ply. For Tsai-Wu criteria, the

optimizer recommends the exact same plies as using stress-based criteria.

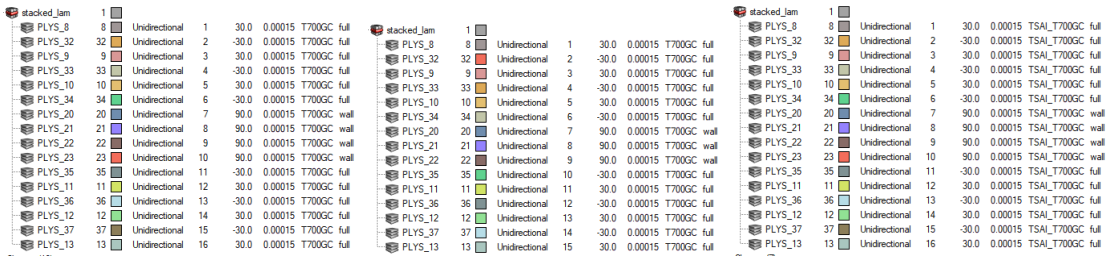

Figure 3.11: Final stack layup for the Traditional Approach. From left to right is the Stress-Based Criterion (16 total plies) $[(\pm 30)_3, 90_2]_s$, Max Strain Criterion (15 total plies) $[(\pm 30)_3, 90, \overline{90}]_s$, and Tsai-Wu (16 total plies) $[(\pm 30)_3, 90_2]_s$.

For the Traditional Approach, each failure criterion calls for almost the exact same layup. For Stress-Based Criteria, the total output mass is about 19.1 kg, as is the mass for Tsai-Wu. For Max Strain, the total mass is about 18.4 kg. Looking at the resultant stresses, the maximum axial stress is about 164 MPa for the Stress-Based and Tsai-Wu criteria, whereas the Max Strain Criteria has a maximum axial stress of 204 MPa, as seen at the top of figure 3.12. The minimum axial stress occurs at the domes at about ~ 55 MPa, much more than the dome stress for the 0°-Band Approach. These again are all very well within the allowable stress. The resultant maximum hoop stress are all $\sim 48 - 49$ MPa seen at the bottom of figure 3.12. The failure indices can also be looked at in figure 3.13 and are all below a failure value of 1.0.

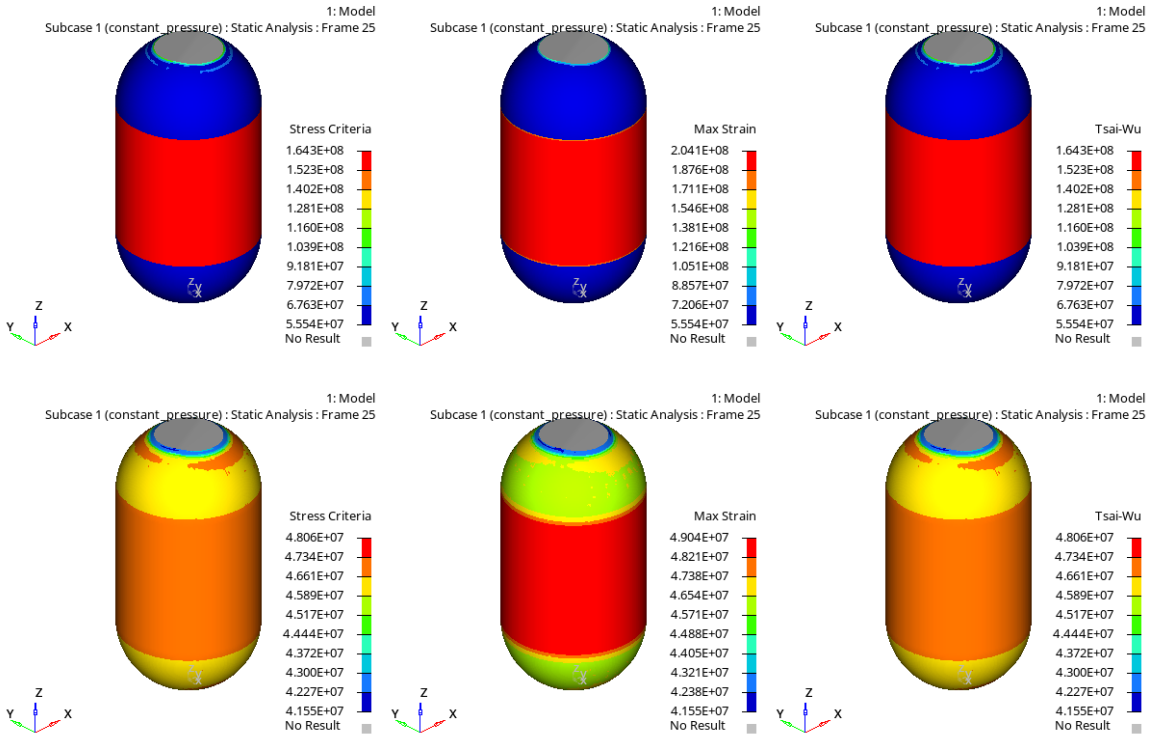

Figure 3.12: Final axial stress on top and final hoop stress on bottom for the Traditional Approach without the 0°-band [Pa]. Notice how the stress in the domes are larger than the dome stresses in figure 3.8 in either the hoop or axial directions.

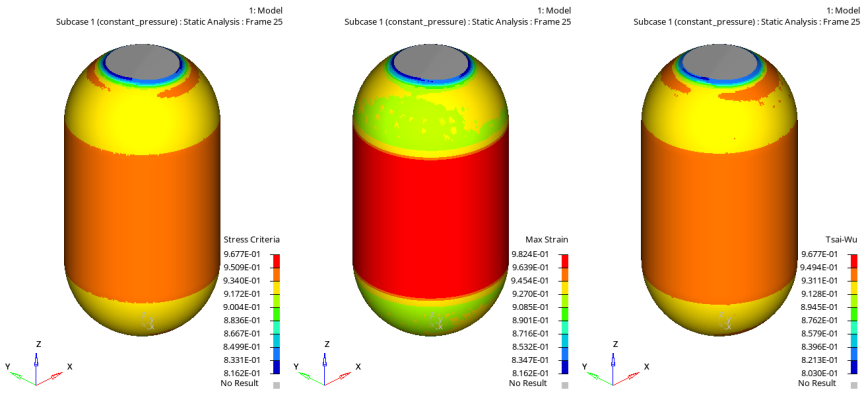

Figure 3.13: Final failure indices for the Traditional Approach.

3.3.3 The Quasi-Isotropic Approach

Before reordering the plies, the axial and hoop stresses can be analyzed to ensure the resultant stresses are within the allowable maximum stresses. As seen on the top half of figure 3.14, for each criterion the maximum axial stress is at the walls of the tank as with the other two approaches. The same is true in the hoop direction, as seen at the bottom half of figure 3.14. The hoop stress also falls within the maximum allowable hoop stress, verifying that the optimization was done correctly.

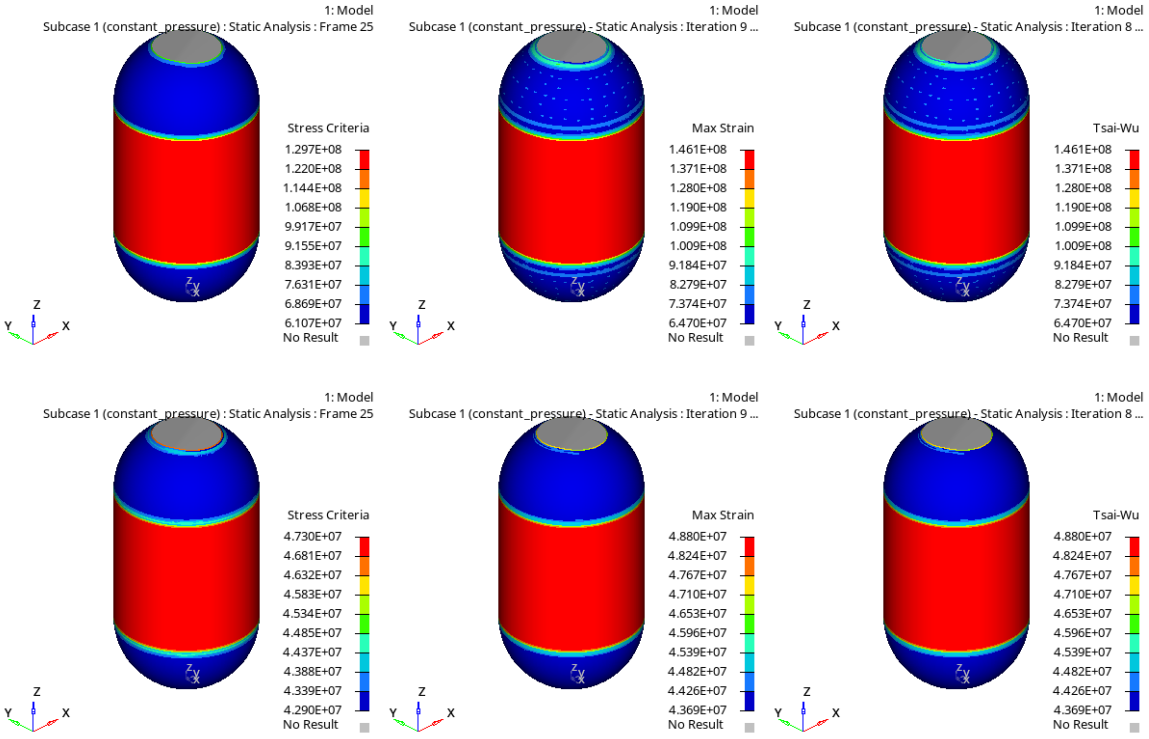

Figure 3.14: Axial stress for the Quasi-Isotropic Approach on top and hoop stress for the Quasi-Isotropic Approach on the bottom [Pa], before balancing the laminate stack.

Once the optimization is verified to have been done correctly, the final stacks can be made for each failure criterion as seen in figure 3.7. For Stress-Based Criteria, the optimizer recommends two plies each of $\pm 45°$, seven $90°$plies, and two $0°$plies. For Max Strain Criteria, the optimizer recommends the same amount of plies, except one less $90°$ply. For Tsai-Wu

criteria, the optimizer recommends the exact same plies as using Max Strain Criteria.

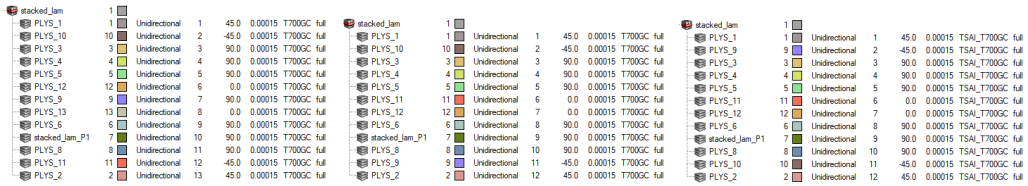

Figure 3.15: Final stack layup for the Quasi-Isotropic Approach. From left to right is the Stress-Based Criterion (13 total plies) $[(\pm 45), 90_3, 0, \overline{90}]_s$, Max Strain Criterion (12 total plies) $[(\pm 45), 90_3, 0]_s$, and Tsai-Wu (12 total plies) $[(\pm 45), 90_3, 0]_s$.

For the Quasi-Isotropic Approach, each failure criterion calls for almost the exact same layup. For Stress-Based Criteria, the total output mass is about 17.6 kg. For Max Strain, the total mass is about 16.3 kg as is for Tsai-Wu. Looking at the resultant stresses, the maximum axial stress is about 130 MPa for the Stress-Based Criteria whereas the Max Strain and Tsai-Wu Criteria has a maximum axial stress of 146 MPa, as seen at the top of figure 3.16. The minimum axial stress occurs at the domes at about $\sim 61 - 71$ MPa, much more than the dome stress for the 0°-Band Approach and even more than the Traditional Approach. These again are all very well within the allowable stress. The resultant maximum hoop stress are all $\sim 47 - 48$ MPa seen at the bottom of figure 3.16, comparable to the Traditional Approach. The failure indices can also be looked at in figure 3.17 and are all below a failure value of 1.0.

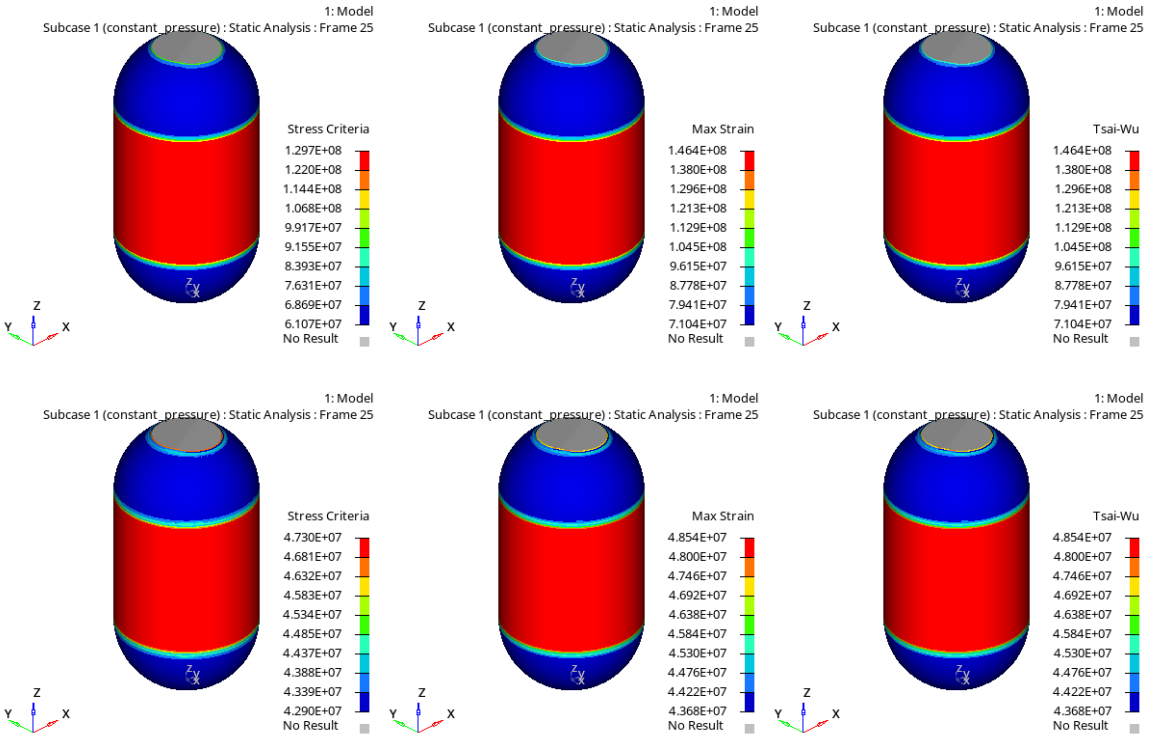

Figure 3.16: Final axial stress on top and final hoop stress on bottom for the Quasi-Isotropic Approach [Pa]. Notice how the stress in the domes are larger than the dome stresses in figure 3.8 in either the hoop or axial directions.

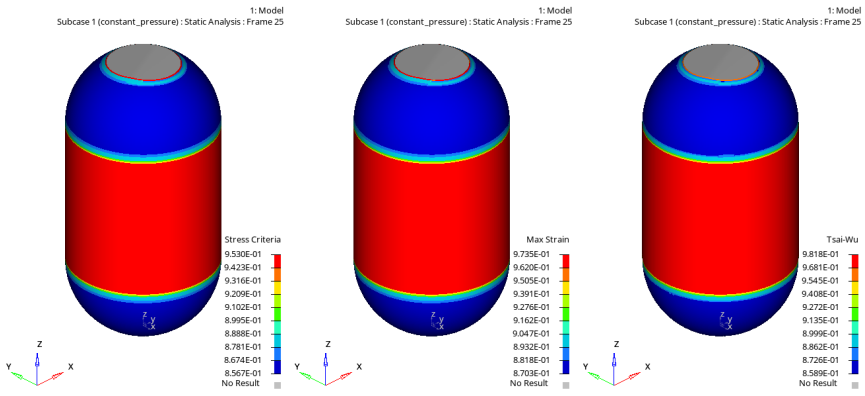

Figure 3.17: Final failure indices for the Quasi-Isotropic Approach.

3.4 Benchmark Industry Quasi-Isotropic Approach

The different models need to be compared with one another as well as a benchmark model that may be seen in industry under the same loading conditions. To do this, a linear static quasi-isotropic model is made where the final stack makes the model just strong enough to withstand the loading conditions present in the optimized models. This was done for every failure criterion and each result yielded the same stacking sequence and final stresses. The final stack can be seen in figure 3.18 and right away, it is apparent that compared to the optimized Quasi-Isotropic Approach, an extra three to four plies are needed. Right away the structural importance of the 90°plies, which there are more of in the optimized model, shines over the ±45° plies.

stacked_lam	1						
stacked_lam_P4	32	Unidirectional	1	0.0	0.00015	T700GC	full
stacked_lam_P1	7	Unidirectional	2	45.0	0.00015	T700GC	full
stacked_lam_P3	31	Unidirectional	3	-45.0	0.00015	T700GC	full
stacked_lam_P2	19	Unidirectional	4	90.0	0.00015	T700GC	full
ply1	33	Unidirectional	5	90.0	0.00015	T700GC	full
ply2	34	Unidirectional	6	-45.0	0.00015	T700GC	full
ply3	35	Unidirectional	7	45.0	0.00015	T700GC	full
ply4	36	Unidirectional	8	0.0	0.00015	T700GC	full
ply5	37	Unidirectional	9	0.0	0.00015	T700GC	full
ply6	38	Unidirectional	10	45.0	0.00015	T700GC	full
ply7	39	Unidirectional	11	-45.0	0.00015	T700GC	full
ply8	40	Unidirectional	12	90.0	0.00015	T700GC	full
ply9	41	Unidirectional	13	90.0	0.00015	T700GC	full
ply10	42	Unidirectional	14	-45.0	0.00015	T700GC	full
ply11	43	Unidirectional	15	45.0	0.00015	T700GC	full
ply12	44	Unidirectional	16	0.0	0.00015	T700GC	full

Figure 3.18: Final layup for the Benchmark Industry Quasi-Isotropic model (16 plies) $[0, (\pm 45), 90]_{4s}$.

For this approach, the total output mass is 21.7 kg, which is more than every other opti-

mized case except the 0°-Band Approach. Looking at the resultant stresses, the maximum axial stress is about 142.5 MPa at the cylinder walls and the minimum stresses occur at the domes as expected, 37 MPa axially and 41 MPa in the hoop direction. While these stress values are comparable to the optimized Quasi-Isotropic Approach, the weight gain is significant, especially once the steel plates are taken into account. A simpler way to compare these two models is to look at the amount of plies since they both use the exact same ply shapes, so the weight percent difference will correspond with the material percent difference. Using 16 plies as opposed to 12 plies accounts for using 28.5% less material when looking at the material percent difference. When scaled up, these weight savings can account for thousands of dollars of rocket fuel not needed.

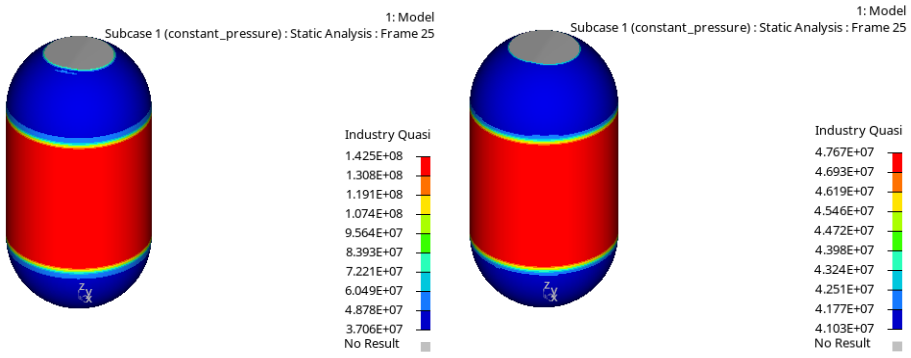

Figure 3.19: Final axial stress on the left and final hoop stress on the right for the Benchmark Industry Quasi-Isotropic Approach [Pa].

3.5 Inquiry into Manufacturability

While strength and mass are integral to creating an optimal layup in any composite-based structure, other manufacturing constraints and considerations need to be taken into account. Thanks to Kameron Harmon, Lab Manager of the Advanced Composite Center in Seattle, Washington, we are able to do just that. Using CGTech's VCP/VCS, Kameron was able to simulate these three design approaches to verify their ability to be manufactured using ElectroImpact's AFP 4.0 machine much like the one in figure 1.5 in chapter one. The tank

being simulated by Kameron in VCS is shown in figure 3.20.

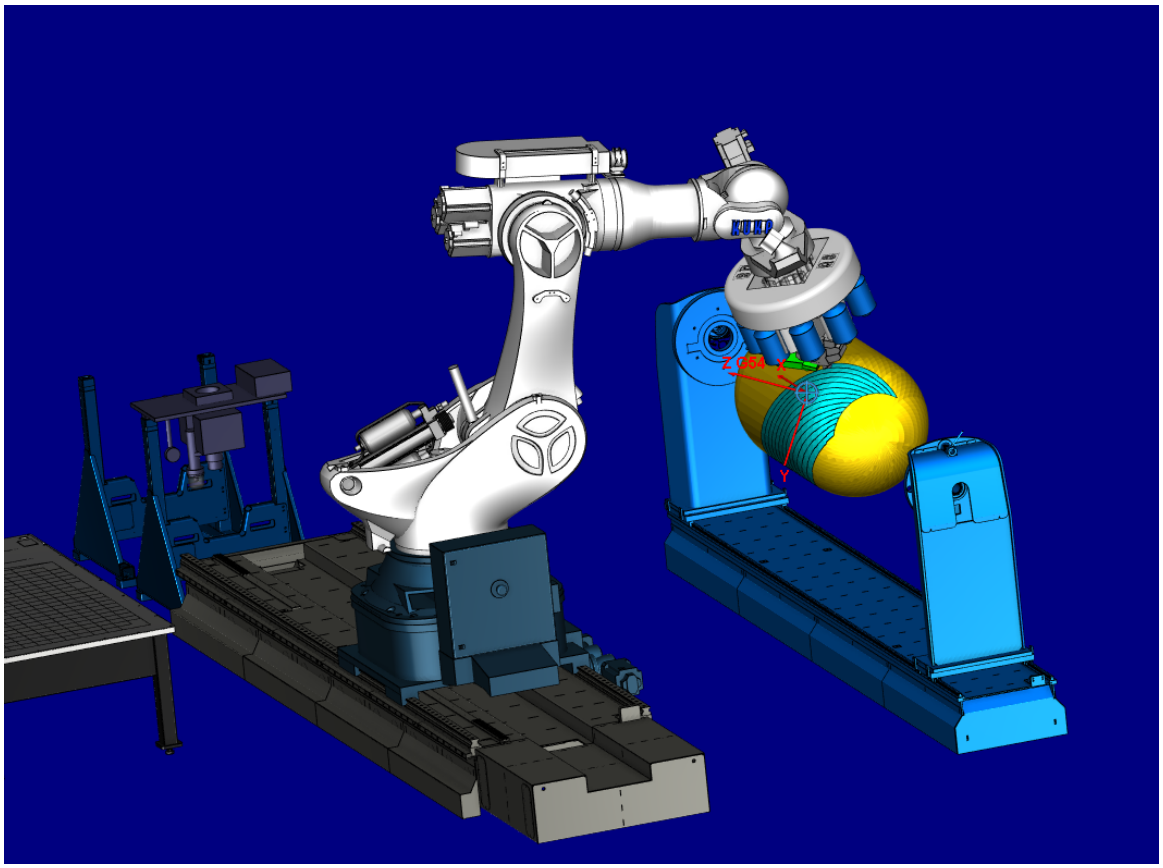

Figure 3.20: Screenshot of the VCS simulation for the ElectroImpact AFP 4.0 machine laying 30°tows (teal strips) on the tool (yellow cylinder).

An important manufacturing constraint to note is this particular AFP robot has a minimum tow length of $\sim 100mm$, which is slightly shorter than the 0_5 band tow length. This can be adjusted by making every 0°band slightly longer to make the 0_5 band fit to minimum tow length requirements. The difference that would need to be made up is $\sim 20mm$. Another note on this minimum tow length is this tank is somewhat smaller than some other cryotanks used for space-based applications, such as the ones in figure 1.7. For scaled-up tanks, this would no longer be an issue, since scaling this model up by just 1.25x is enough to make the 0_5 band meet minimum tow length requirements.

3.5.1 Manufacturing Times

One manufacturing consideration that must be taken into account is the time it takes for the Advanced Fiber Placement (AFP) machine to make the cryotank for each design approach. Kameron simulated the times is takes for the AFP 4.0 machine to make the full shape for 0°, 30°, and 90°plies, the wall shape for 90°plies, and the 0_1 and 0_4 bands. Not all the shapes were simulated but they are enough information for a time study. Some simple calculations can be taken for an approximate total manufacturing time, taking note that the 0°band simulations include a band on the top and bottom. Some approximations are taken, first that the full shape 45°plies are close enough to full shape 30°plies so similar manufacturing times are taken. For the other 0°-bands, the $0\_2 = 8{:}30, 0\_3 = 6{:}30, 0\_5 = 5{:}00$ manufacturing times. These are just approximations base done what is given. Lastly, manufacturing continuous 90°plies are very time consuming, so often they are manufactured as highly helical plies. They have almost the exact same properties as 90°plies as the ones that are simulated, but this is a technique often used to save time and is used by Kameron to give more realistic results for both the full and wall shapes.

Column1	Time (H:MM:SS)	Time Laying Tape	Time On-Part	Time Off-Part	On-Part %	Off-Part %
Sequence 1	0:49:36					
Machine 1	0:49:36	0:24:25	0:28:09	0:21:27	56.8	43.2
Ply 1- Full 0Deg	0:12:37	0:05:27	0:06:04	0:06:32	48.1	51.9
Ply 2- Full 90Deg	0:07:00	0:06:49	0:06:50	0:00:10	97.6	2.4
Ply 3-0Band_4	0:05:37	0:01:05	0:02:11	0:03:26	38.9	61.1
Ply 4-0Band_1	0:09:48	0:02:47	0:03:56	0:05:52	40.2	59.8
Ply 5- 90Deg Cylinder	0:03:53	0:03:43	0:03:44	0:00:09	96.3	3.7
Ply 6-Full 30Deg	0:10:40	0:04:34	0:05:23	0:05:18	50.4	49.6
Total	0:49:36					

Figure 3.21: Manufacturing timetable courtesy of Kameron Harmon.

The approximate manufacturing times for each approach and failure criteria is tabulated below in table 3.1. The times for each manufacturing approach is similar regardless of their failure criteria, however, the optimized Quasi-Isotropic Approach is by far the quickest to manufacture compared to the other two approaches. This is thanks to the manufacturing trick to change 90°plies to $\sim 88°$ plies which significantly cuts down on time. While the trick was also used for the 90°wall shape, the optimized Quasi-Isotropic Approach uses so many 90°plies compared to every other approach that the most time was saved using this design approach.

Manufacturing Times, hr:min:sec				
Failure Criteria	0°-Band	Traditional	Quasi-Isotropic	Benchmark
Stress-Based	3:08:45 (+14.2%)	2:23:32 (-13.2%)	1:56:54 (-33.4%)	2:43:48
Max Strain	3:18:33 (+19.2%)	2:18:39 (-16.6%)	1:49:54 (-39.4%)	-
Tsai-Wu	3:08:45 (+14.2%)	2:23:32 (-13.2%)	1:49:54 (-39.4%)	-

Table 3.1: Approximate manufacturing times and their percent savings for each layup depending on approach and failure criteria. Since the Benchmark is not optimized, only one manufacturing time is reported and the other fields are blank.

Chapter 4

CONCLUSION

While many cryogenic propellant tanks are made of carbon fiber reinforced composite material (CFRC) nowadays, few are made and optimized to be as simple as possible with no extra support structures. By making the tank as simple as possible while still being able to withstand the forces and extreme temperatures to hold the LH2 propellant efficiently, weight can be significantly cut and thus save a lot of money in terms of rocket fuel needed.

Total mass outputs for every optimized model as well as the non-optimized Benchmark Industry model are seen in table 4.1. For every case except the 0°-Band Approach, optimizing the cryotank allows for mass savings. The reason the 0°-band is heavier is due to the extra reinforcement in the domes. For the most apples-to-apples comparison, the optimized Quasi-Isotropic Approach can be compared to the non-optimized Benchmark Quasi-Isotropic Approach since they are the exact same approaches, but one is optimized while the Benchmark is not. As seen in table 4.1, there is clear mass savings due to this optimization strategy that can save as much as 28.4% difference in final structure mass.

Masses, [kg]				
Failure Criteria	0°-Band	Traditional	Quasi-Isotropic	Benchmark
Stress-Based	23.4 (+7.5%)	19.1 (-12.7%)	17.6 (-20.9%)	21.7
Max Strain	24.5 (+12.1%)	18.4 (-16.5%)	16.3 (-28.4%)	-
Tsai-Wu	23.4 (+7.5%)	19.1 (-12.7%)	16.3 (-28.4%)	-

Table 4.1: Masses and their percent savings compared to the Benchmark for each optimized design approach. Since the Benchmark is not optimized, only one mass is reported and the other fields are blank.

Maximum thickness can also be analyzed to understand material savings in different

areas of the cryotank. Comparatively, the optimized Quasi-Isotropic Approach used the least amount of material all-around, whereas the 0°-Band Approach used the most all around. This is also apparent from the output masses.

Thicknesses, [mm]				
	0°-Band	Traditional	Quasi-Isotropic	Benchmark
Walls	2.4	2.25-2.4	1.8-1.95	2.4
Domes	2.7-2.85	1.8	-	-

Table 4.2: Maximum thicknesses for each design approach. For the 0°-Band Approach, the band ranges from 0.9-1.05 mm added on top if its dome thickness depending on failure criterion used. The Quasi-Isotropic Approach and the Benchmark is only full shapes, so the wall thickness is the entire thickness, since it is continuous in thickness all around.

Comparing between the different approaches, mass savings of 2-7 kilograms are possible with the lightest tank being from the optimized Quasi-Isotropic Approach. If saving as much mass as possible is the goal of the manufacturer, then the optimized Quasi-Isotropic Approach saves the most mass. That being said, with the manufacturing tricks used, the optimized Quasi-Isotropic Approach is significantly faster than the 0°-Band Approach, and is still about 20-30 minutes faster than the Traditional Approach and Benchmark. By optimizing the Benchmark Approach, the manufacturing time can be cut by over one-third.

For hoop stresses, the maximum occurs for every model at the walls and are all about the same. However, the 0°-Band Approach significantly decreases hoop stress in the domes, with the other two optimized approaches having similar hoop stresses at the domes with each other and with the Benchmark. For axial stresses, almost every model has comparable maximum stress at the walls. However, once again in the dome the 0°-Band Approach is significantly less than the other two approaches. So in terms of stresses, if there is concern for failure in the domes then the 0°-Band Approach is superior to all approaches.

Overall, each approach has its own benefits. The 0°-Band Approach takes the longest to make, but it is the best at distributing stresses. The Quasi-Isotropic Approach is the

lightest and fastest to make, but it is not as strong as the other approaches. Then there is the Traditional Approach, which is middle of the pack in just about every category. It is better at distributing stresses in the walls but not the domes than the Quasi-Isotropic Approach, showing how well the 0°-band eases stress in the domes. There is not a clear winner in which design is best, that is up to the manufacturer based on mission and savings goals. For the most apples-to-apples comparison, the Optimized Quasi-Isotropic model used less helical plies and more hoops compared to the Benchmark and because of this, saved weight and manufacturing time. If more benchmarks were made for approaches such as the Traditional Approach, the results would likely be the same. No matter what, the most likely area of failure occurs at the cylinder walls, so the approach that best supports the walls and not so much the domes is likely to be the best.

4.1 Future Work

This cryotank study and the overall process can be improved upon. First, before doing any modelling, it is helpful to do preliminary hand calculations to understand a ballpark of what a reasonable answer may be. For example, simple hand calculations for hoop and axial stress can be performed to understand how many plies we may expect given our material. For the hoop stress, we can solve the hoop stress of a pressure vessel for wall thickness to be,

$$t = \frac{PD}{(2\sigma_\theta + P)} \tag{4.1}$$

where P is internal pressure (0.375 MPa for this tank with FOS of 1.5), D is the diameter (1.0 m), σ_θ is the allowable stress in the fiber direction (2167.623 MPa). For the axial stress of a pressure vessel, it is simply,

$$t = \frac{PD}{(4\sigma_\theta + P)} \tag{4.2}$$

For this tank, the thickness came out to be less than a single ply. This does not include the temperature effects. If these hand calculations were done prior to building the model, time would have been saved by seeing just how important the temperature effect is and it

would have been added at the start, rather than having to redo everything much later on in the project. This would have led to a study that goes just a little bit deeper or more complex.

An important improvement to this study is the process in which the optimization was done itself. From the second optimization, the optimization that looked at shapes, too few shape ideas came out to allow the optimizer to shine. Instead of proposing one shape that tapers in, as seen in the 0°-band, many more shapes should have been used in conjunction with more human interpretation. While the 0°-band was a good start, many more shapes should have been used that converged towards different areas of the tank. These shapes could have been from the ends converging towards the center of the cylinder, or from the center of the cylinder converging towards the dome-ends, etc. Once running the third optimization with all of these shapes, it would then be up to the interpreter on which shapes were the most useful, much like the results of the first optimization. A quick example was made after-the-fact to prove how the optimizer would work better with this method. The optimized Quasi-Isotropic Approach was made the exact same as for the third optimization, but now another shape was introduced that was just a little bit longer than the cylindrical walls, as seen in figure 4.1.

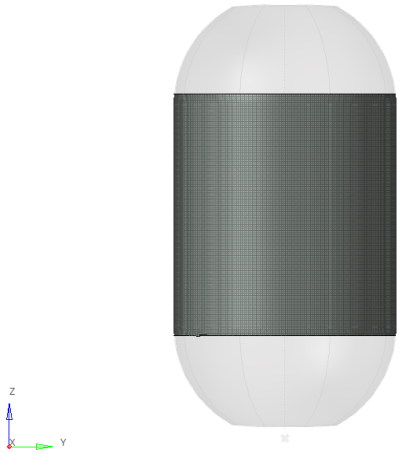

Figure 4.1: Shape made that is just a little longer than the walls for the after-the-fact quasi-isotropic model.

When run using the third optimization strategy, the optimizer chose a few plies of the new 90°shape (named 90_b) in place of some of the full-shaped 90°plies. The final output had a mass of 18.6 kg and a layup code $[(\pm 45), 90_2, 0_2, 90_b, \overline{90_b}]_s$. Just this quick fix resulted in mass savings of 15.4% compared to the non-optimized Benchmark. If given more options, it is reasonable to assume that the optimizer would have "chosen" few, if any, full 90°shapes saving even more mass. For the manufacturing time, the new 90_b° shape is assumed to take just a little longer than the 90°wall shape. The approximated manufacturing time is 2:21:08, saving 14.9% in manufacturing time compared to the Benchmark. The final stresses of this result also shows that introducing more shapes that vary allows for the maximum stresses to be closer to failure all around, as seen in figure 4.2.

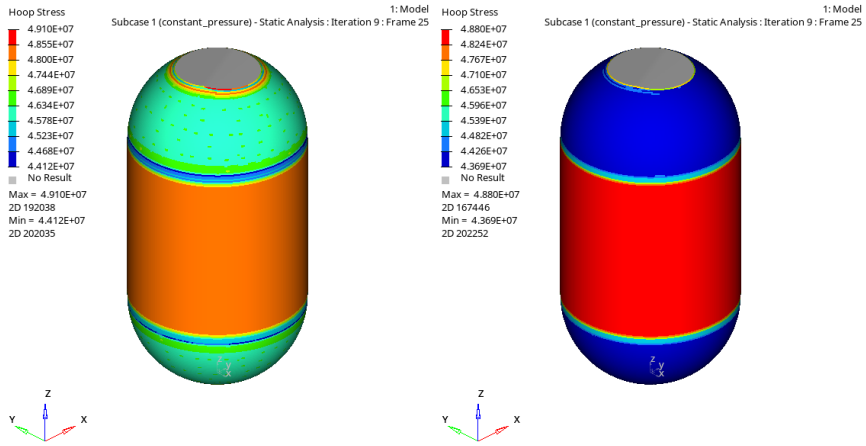

Figure 4.2: Hoop stresses for the after-the-fact optimized quasi-isotropic approach (left) compared to the optimized Quasi-Isotropic Approach (right). Demonstrating the use of more layers would result in likely a more optimized structure.

By being closer to failure all around, this effectively means the optimizer would choose less material in the domes and instead allocate more towards the cylinder walls, since those are what proved themselves to be the driving force of this optimization. The ultimate goal of optimization is to have the entire structure be close to failure all around, not just in one area such as the cylinder walls as was the case in this study. By having the entire structure be close to failure, it means it is made with as little material as is necessary to just not fail

all around. Figure 4.3 proves that given more shape options, the optimizer would do just that. With more layers shapes as the tank on the left has, the maximum failure index is a little lower and the minimum failure index is a little higher compared to the tank on the right.

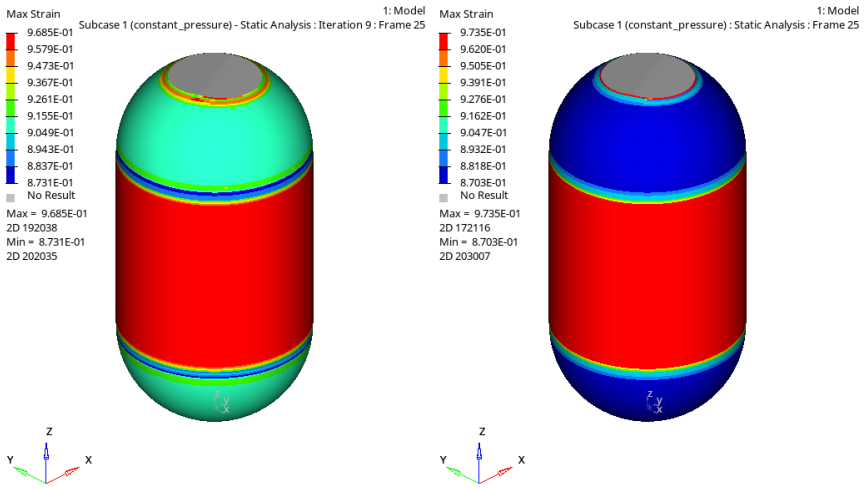

Figure 4.3: Failure indexes for the after-the-fact optimized quasi-isotropic approach (left) compared to the optimized Quasi-Isotropic Approach (right). Demonstrating the use of more layers would result in the failure index converging to failure all around the tank.

Another way to improve upon this study is to also model the liner inside the CFRC layers and the insulation as well. This would likely impact just how much CFRC is used because it can take possible fuel boil off and temperature effects more accurately, rather than by approximation as done here. The liner would need to be modelled with the stacked laminate but since it acts as a "ply," it is paramount that $SMEAR$ is on because it would lead to an unbalanced laminate if left off. The insulation would be modelled by running a linear static analysis to understand the temperature gradient over a specified period of time and then applied when running the program for optimizations and linear static analyses.

Lastly, future studies can include more complex or even simpler cryotanks. Support systems can be accounted for such as the ones in chapter one to find more unique ways to make CFRC cryotanks as light as possible. Or, completely spherical cryotanks can be

studied to completely remove the weak point of this tank, the walls. By making a spherical cryotank, a similar 0°-band can be explored to try reinforcing the tank as much as possible. However, then the size needs to be taken into account. It is one thing to make a cylindrical tank to put on a cylindrical rocket, it's another thing to try to fit a massive sphere inside (or outside) a cylindrical rocket.

BIBLIOGRAPHY

[1] Kwan-Woo Kim, Dong-Kyu Kim, Byoung-Suhk Kim, Kay-Hyeok An, Soo-Jin Park, Kyong Yop Rhee, and Byung-Joo Kim. Cure behaviors and mechanical properties of carbon fiber-reinforced nylon6/epoxy blended matrix composites. *Composites Part B: Engineering*, 2017.

[2] Ni Liu et al. Progress in research on composite cryogenic propellant tank for large aerospace vehicles. *Composites Part A: Applied Science and Manufacturing*, 2021.

[3] Rocket Lab, 2023. Accessed: 2024-05-28.

[4] ElectroImpact, 2024. Accessed: 2024-03-01.

[5] Yadav Khagendra Kumar and Dalbir Lohchab. Influence of aviation fuel on mechanical properties of glass fiber-reinforced plastic composite, 2016. Accessed: 2024-02-21.

[6] Hongfei Zheng, Xuesen Zeng, Jianbao Zhang, and Hongjie Sun. The application of carbon fiber composites in cryotank. *Solidification*, 2018.

[7] C. Barile, C. Casavola, and F. De Cillis. Mechanical comparison of new composite materials for aerospace applications. *Composites Part B: Engineering*, 162:122–128, 2019.

[8] Robert M. Jones. *Mechanics Of Composite Materials (2nd ed.)*. CRC Press, 1999.

[9] NASA. Nasa awards contract for liquid hydrogen. https://www.nasa.gov/news-release/nasa-awards-contract-for-liquid-hydrogen/, 2022. Accessed: 2024-02-20.

[10] NASA. Engineers chill space launch system rocket engines before launch. https://www.nasa.gov/centers-and-facilities/marshall/engineers-chill-space-launch-system-rocket-engines-before-launch/: :text=During Accessed: 2024-02-20.

[11] Wang Wei, Huang Rongjin, Huang Chuanjun, Yuqiang Zhao, Shaopeng Li, and Li Laifeng. Cryogenic performances of t700 and t800 carbon fibre- epoxy laminates. *IOP Conference Series: Materials Science and Engineering*, 102(1):012016, nov 2015.

[12] Douglas A. McCarville, Juan C. Guzman, Alexandra K. Dillon, Justin R. Jackson, and Jordan O. Birkland. 3.5 design, manufacture and test of cryotank components. In Peter W.R. Beaumont and Carl H. Zweben, editors, *Comprehensive Composite Materials II*, pages 153–179. Elsevier, Oxford, 2018.

[13] W. Seneviratne K. S. Raju J. Tomblin, J. Sherraden. A – basis and b – basis design allowables forepoxy – based prepreg toray t700gc-12k-31e/2510 unidirectional tape. Technical report, National Institute for Aviation Research, 2002.

[14] Toray Composite Materials America, Inc. https://www.toraycma.com/products/carbon-fiber/, 2024. Accessed: 2024-05-17.

[15] The Engineering Toolbox. https://www.engineeringtoolbox.com/engineering-materials-properties-d$_1$225.*html*, 2008. *Accessed* : $2024 - 05 - 17$.

[16] Jeffrey A. Wollschlager. *Introduction to the Design and Analysis of Composite Structures An Engineer's Practical Guide Using Optistruct.* Jeffrey A. Wollschlager, 2021.

[17] Zdenek P Bažant, Jia-Liang Le, and Marco Salviato. *Quasibrittle fracture mechanics and size effect: A first course.* Oxford University Press, 2021.

[18] Marco Salviato, Kedar Kirane, Shiva Esna Ashari, Zdeněk P Bažant, and Gianluca Cusatis. Experimental and numerical investigation of intra-laminar energy dissipation and size effect in two-dimensional textile composites. *Composites Science and Technology*, 135:67–75, 2016.

[19] Marco Salviato, Kedar Kirane, Zdeněk P Bažant, and Gianluca Cusatis. Mode i and ii interlaminar fracture in laminated composites: a size effect study. *Journal of Applied Mechanics*, 86(9):091008, 2019.

[20] Marco Salviato, Viet T Chau, Weixin Li, Zdeněk P Bažant, and Gianluca Cusatis. Direct testing of gradual postpeak softening of fracture specimens of fiber composites stabilized by enhanced grip stiffness and mass. *Journal of Applied Mechanics*, 83(11):111003, 2016.

[21] Weixin Li, Yao Qiao, Joel Fenner, Kyle Warren, Marco Salviato, Zdeněk P Bažant, and Gianluca Cusatis. Elastic and fracture behavior of three-dimensional ply-to-ply angle interlock woven composites: Through-thickness, size effect, and multiaxial tests. *Composites Part C: Open Access*, 4:100098, 2021.

[22] Seunghyun Ko, Jinkyu Yang, Mark E Tuttle, and Marco Salviato. Effect of the platelet size on the fracturing behavior and size effect of discontinuous fiber composite structures. *Composite Structures*, 227:111245, 2019.

[23] Seunghyun Ko, James Davey, Sam Douglass, Jinkyu Yang, Mark E Tuttle, and Marco Salviato. Effect of the thickness on the fracturing behavior of discontinuous fiber composite structures. *Composites Part A: Applied Science and Manufacturing*, 125:105520, 2019.

[24] Yao Qiao, Antonio Alessandro Deleo, and Marco Salviato. A study on the multi-axial fatigue failure behavior of notched composite laminates. *Composites Part A: Applied Science and Manufacturing*, 127:105640, 2019.

[25] Yao Qiao and Marco Salviato. Micro-computed tomography analysis of damage in notched composite laminates under multi-axial fatigue. *Composites Part B: Engineering*, 187:107789, 2020.

[26] Yao Qiao, Qiwei Zhang, and Marco Salviato. Effects of in-situ stress state on the plastic deformation, fracture, and size scaling of thermoset polymers and related fiber-reinforced composites. In *Proceedings to 35th Annual Technical Conference on Composite Materials*, 2020.

[27] Yao Qiao, Qiwei Zhang, TROY Nakagawa, and MARCO Salviato. A size effect study on the splitting crack initiation and propagation in off-axis layers of composite laminates. In *36th American Society for Composites Conference*, 2021.

[28] Yao Qiao, Kaiwen Guo, and Marco Salviato. Size effect and scaling in quasi-static and fatigue fracture of graphene polymer nanocomposites. *Polymer Composites*, 2023.

[29] Yao Qiao and Marco Salviato. Strength and cohesive behavior of thermoset polymers at the microscale: A size-effect study. *Engineering Fracture Mechanics*, 213:100–117, 2019.

[30] Yao Qiao and Marco Salviato. Study of the fracturing behavior of thermoset polymer nanocomposites via cohesive zone modeling. *Composite Structures*, 220:127–147, 2019.

[31] Jeremy Brockmann and Marco Salviato. The gap test–effects of crack parallel compression on fracture in carbon fiber composites. *Composites Part A: Applied Science and Manufacturing*, 164:107252, 2023.

[32] Kedar Kirane, Marco Salviato, and Zdeněk P Bažant. Microplane triad model for simple and accurate prediction of orthotropic elastic constants of woven fabric composites. *Journal of Composite Materials*, 50(9):1247–1260, 2016.

[33] Marco Salviato, Shiva Esna Ashari, and Gianluca Cusatis. Spectral stiffness microplane model for damage and fracture of textile composites. *Composite Structures*, 137:170–184, 2016.

[34] Kedar Kirane, Marco Salviato, and Zdeněk P Bažant. Microplane-triad model for elastic and fracturing behavior of woven composites. *Journal of Applied Mechanics*, 83(4):041006, 2016.

[35] Yuta Kumagai, Sota Onodera, Marco Salviato, and Tomonaga Okabe. Multiscale analysis and experimental validation of crack initiation in quasi-isotropic laminates. *International Journal of Solids and Structures*, 193:172–191, 2020.

[36] Yuval Freed, Marco Salviato, and Navid Zobeiry. Implementation of a probabilistic machine learning strategy for failure predictions of adhesively bonded joints using cohesive zone modeling. *International Journal of Adhesion and Adhesives*, 118:103226, 2022.

[37] Yuval Freed, Navid Zobeiry, and Marco Salviato. Development of aviation industry-oriented methodology for failure predictions of brittle bonded joints using probabilistic machine learning. *Composite Structures*, 297:115979, 2022.

[38] Seunghyun Ko, Troy Nakagawa, Zhisong Chen, William B Avery, Ebonni J Adams, Matthew R Soja, Michael H Larson, Chul Y Park, Jinkyu Yang, and Marco Salviato. Effects of average number of platelets through the thickness and platelet width on the mechanical properties of discontinuous fiber composites. *Composites Part A: Applied Science and Manufacturing*, 177:107945, 2024.

[39] MARCO SALVIATO, SEAN E PHENISEE, ANTONIO A DELEO, DANIELE PELESSONE, and MARK FLORES. To the mesoscale and beyond! capturing complex damage mechanisms in composites via simple, physics-based, discrete mathematical models of fibers and matrix. In *PROCEEDINGS OF THE AMERICAN SOCIETY FOR COMPOSITES-THIRTY-EIGHTH TECHNICAL CONFERENCE*, 2023.

[40] Marco Salviato, Sean Phenisee, Antonio Deleo, Daniele Pelessone, and Mark Flores. A novel discrete, mesoscale modeling framework for the simulation of the damaging and fracturing behavior of composites. In *ASME International Mechanical Engineering Congress and Exposition*, volume 86717, page V009T12A015. American Society of Mechanical Engineers, 2022.

[41] Seunghyun Ko, Kenrick Chan, Reed Hawkins, Rohith Jayaram, Christopher Lynch, Reda El Mamoune, Minh Nguyen, Nicolay Pekhotin, Natania Stokes, D Wu, et al. Experimental and numerical characterization of the intra-laminar fracturing behavior in discontinuous fiber composite structures. In *Proceedings of the 33th ASC conference, Seattle, WA, USA*, pages 24–26, 2018.

[42] Subodh K. Mital et al. Review of current state of the art and key design issues with potential solutions for liquid hydrogen cryogenic storage tank structures for aircraft applications. Technical report, NASA, 2006.

[43] NASA. Launch day play-by-play. https://www.nasa.gov/wp-content/uploads/2020/02/ppt$_l aunch_d ay_p lay - by - play_d m - 2_5 08.pdf?emrc = 17cf30, 2020. Accessed : 2024 - 05 - 18.$

[44] George H. Staab. 6 - laminate analysis. In George H. Staab, editor, *Laminar Composites*, pages 191–282. Butterworth-Heinemann, Woburn, 1999.